ErbB2/HER2 expression level determines CDK4-inhibitor sensitivity and cyclin D1 and c-Myc dependency at the G1/S transition

Authors: Ayaka Nagasato-Ichikawa[1], Ken Murakami[1], Kazuhiro Aoki[2,3], Mariko Okada[1]*

Affiliations:

[1]Laboratory for Cell Systems, Institute for Protein Research, Osaka University, Suita, Osaka, 565-0871, Japan

[2]Exploratory Research Center on Life and Living Systems (ExCELLS), National Institutes of Natural Sciences, Okazaki, Japan; National Institute for Basic Biology, National Institutes of Natural Sciences, Okazaki, Japan; Department of Basic Biology, School of Life Science, SOKENDAI (The Graduate University for Advanced Studies), Okazaki, 44-8787, Japan

[3]Graduate School of Biostudies, Kyoto University, Kyoto, 606-8501, Japan.

*Corresponding author: mokada@protein.osaka-u.ac.jp

Bullet points

1. After ErbB2 activation, G1/S transition was driven by CDK4-cyclin D1 activity.
2. Most cells were arrested in the G1 phase after CDK4 inhibition, but cells with increased c-Myc transcriptional activity were insensitive to CDK4 inhibition.
3. Hsp90-mediated ErbB2 stabilization was required for the G1/S transition.
4. High levels of ErbB2 activate AKT and c-Myc and suppress p27 expression, resulting in the accumulation of cyclin D1-CDK4 and cell-cycle arrest.
5. Cells with high ErbB2 expression maintained c-Myc transcriptional activity after CDK4-inhibitor treatment, exhibiting reversible cell-cycle arrest and reduced sensitivity to the inhibitor.

Abstract

Cell-cycle entry and subsequent G1 to S phase transition are crucial for mammalian cell proliferation. The pathway mediated by members of the ErbB receptor family (ErbB1/2/3/4) plays an important role in the proliferation of several types of human cancer cells, and increased ErbB2/HER2 activity is often observed in malignant breast cancer. However, the underlying mechanisms, such as the transcriptional regulation of the G1/S transition via ErbB2 activation, remain unclear. Here, we performed a comprehensive time-course analysis of growth factor-stimulated MCF-7 breast cancer cells to identify the regulatory mechanisms underlying G1/S transition. Live-cell imaging using cell-cycle reporters enabled the estimation of the timing and duration of G1/S transition under conditions of ErbB2 activation, which was found to be mainly driven by cyclin D1/CDK4 under conditions of Hsp90-mediated ErbB2 stabilization. Although most cells exhibited a cell-cycle arrest upon CDK4-inhibitor treatment, a subpopulation of cells exhibited persistent G1/S transition, which was attributed to the activation of the transcriptional activity of c-Myc through epigenetic modifications. Conversely, in cells with high ErbB2-expression, CDK4 inhibition led to an excessive increase in c-Myc transcriptional activity, rapid decrease in cyclin D1 expression, and a reversible cell-cycle arrest. Overall, our results demonstrated that ErbB2 receptor levels alter the dependency of the G1/S regulatory network on cyclin D1 and c-Myc via epigenetic regulation, ultimately providing two routes for cell-cycle progression. These results might be extrapolated to suggest that the differences in ErbB2 levels within breast cancer tissues are associated with heterogeneity in CDK4-inhibitor sensitivity, potentially complicating treatment strategies.

One Sentence Summary: CDK4 inhibition in the background of high ErbB2 expression caused c-Myc activation and reversible cell-cycle arrest.

INTRODUCTION

The initiation of the cell cycle and the subsequent transition from the G1 to S phase involve an intricate network associated with the CDK4/cyclin D1 complex (*1–3*). Understanding the regulation of the G1/S transition by mitogenic signals is fundamental in the field of cell biology and essential for developing cancer treatments and overcoming drug resistance. Cyclin D1 overexpression results in enhanced breast cancer cell proliferation (*4*). Consequently, cell-cycle inhibitors targeting CDK4, a binding partner of cyclin D1, have been developed to treat breast cancer (*5*, *6*). Breast cancer is classified into four subtypes (luminal A, luminal B, ErbB2/HER2 positive, and triple-negative) based on differences in the expression of estrogen receptors (ERs), progesterone receptors (PRs), and ErbB2 (HER2) receptors (*7–9*). CDK4 inhibitors (CDK4is) are used to treat luminal A subtype (ER^+ and $HER2^-$) breast cancers (*5*, *10*). Meanwhile, long-term administration of CDK4is has been linked to treatment resistance and decreased drug sensitivity via pathways such as PI3K/AKT/mTOR and Hippo signaling and non-coding RNA regulation (*11–21*). Therefore, it is important to focus on the mechanism of the G1/S transition after CDK4is treatment, as this will help to elucidate the underlying causes of cell cycle regulation. On the other hand, increased activity of the ErbB2 receptor tyrosine kinase is often found in malignant breast cancer, and ErbB2 increases cyclin D1 levels (*22*, *23*). In addition, it has been reported that a significant subset of ErbB2-overexpressing cells is found in the luminal A subtype, which is typically characterized by relatively low ErbB2 expression (*24*). However, the mechanisms by which changes in ErbB2 expression govern the G1/S transition remain unclear, and the sensitivity of the ErbB2-positive subpopulation (within the luminal A subtype) toward CDK4is is not yet understood.

ErbB receptors can be categorized into four families, i.e., ErbB1 (EGFR), ErbB2 (HER2), ErbB3, and ErbB4. Upon ligand stimulation, each ErbB receptor forms homodimers or heterodimers with other ErbB receptors (*25*, *26*). Activation of ErbB2 receptors results in the activation of the MAPK/ERK and PI3K/AKT pathways, causing rapid expression of early-response genes (ERGs), including c-Fos and c-Myc (*27–29*), which regulate the expression of cell-cycle regulators, such as cyclin D1 and CDK4 (*29–31*). However, c-Myc and cyclin D1 seemingly play different roles in regulating the G1/S transition (*32*), which typically involves a combination of signal-dependent and signal-independent regulation of key transcription factors, i.e., 1) phosphorylation and inactivation of retinoblastoma (RB), a repressor of E2F1, and 2) E2F1-mediated expression of cell-cycle regulators. It is worth noting that there is a boundary between points 1) and 2), which is known as the restriction point (R point) (*2*, *33*). Prior to the R point, the expression and activation of cyclin D1/CDK4 are primarily governed by mitogenic signals that phosphorylate RB. After the R point, E2F1 dissociates from phosphorylated RB (p-RB), leading to increased expression of E2F1-target genes, including cyclin E. Subsequently, cyclin E/CDK2 phosphorylates p-RB (pp-RB), releasing E2F1 (and activating) from pp-Rb. As E2F1 promotes the expression of cyclin E and related genes, the cyclin E/CDK2-RB-E2F1

positive feedback loop is believed to operate independently of mitogenic signals. c-Myc directly affects E2F1 promoter activity, thereby promoting cyclin E and E2F1 expression. Thus, c-Myc, whose expression and stability are controlled by external signals, significantly contributes to the promotion of cyclin E/CDK2-RB-E2F1 feedback regulation after the R point. Cyclin D1/CDK4 is required to maintain the inactivation of RB even after the R point, suggesting its relevance in the progression of the cell cycle from the G1 to the G2 phase (*34*).

Under the ErbB2 activation, both c-Myc and cyclin D1 gene expression and protein stabilization are induced via ERK and AKT activity. On the other hand, however, *p27*mRNA levels, which are important for the accumulation of cyclin D1 and CDK4 during G1 phase, are known to be repressed by c-Myc (*35*). The relationship between c-Myc and cyclin D1 is one in which either expression state is likely to be biased, suggesting that different ErbB2 levels may alter the dependence of cyclin D1 and c-Myc on G1/S transition regulation. It is also known that phosphorylation of c-Myc (Ser^{62}) increases the stability of c-Myc (*36*). In other words, examining the ratio of p-c-Myc to cyclin D1 at the single-cell level could provide important clues as to which pathway is dependent on, and may reveal detailed mechanisms depending on ErbB2 levels. However, the mechanisms underlying the ErbB2-mediated modulation of the activity of cyclin D1/CDK4 and c-Myc, the timing or duration of the G1/S transition and cell-cycle phases, and how ErbB2 expression affects sensitivity to CDK4is remain elusive. Elucidating this mechanism is critical for clarifying the bottleneck in CDK4i therapy and enhancing the efficacy of CDK4is in the treatment of breast cancer.

In the present study, we used representative luminal A subtype cell line (MCF-7), which express low levels of ErbB1 receptor (EGFR) and high levels of the ErbB3 receptor (*29*, *37*). ErbB2 is an orphan receptor that is activated by heterodimerization with activated ErbB3, ErbB4, or EGFR (*28*). Thus, stimulation with the ErbB3 ligand, heregulin (HRG), rather than the EGFR ligand (EGF), triggers stronger signal activity. We conducted a time-course comprehensive analysis by employing transcriptome analysis, epigenetic modification analysis, and live-cell imaging to quantitatively analyze the cell cycle and thoroughly assess the signaling mechanisms (from gene expression to cell-cycle entry) after ErbB2 receptor activation with HRG. Ultimately, we analyzed the differences in ErbB2 expression patterns to investigate how they affect the regulation of the G1/S transition and alter the sensitivity to CDK4is using MCF-7 cells with different ErbB2 expression levels as a breast cancer model.

RESULTS

G1/S transition occurs approximately 20 h after ligand stimulation

First, we investigated the timing of cell-cycle transition in the ErbB signaling pathway. To analyze the cell-cycle dynamics, we established a live-cell imaging analysis system in which the fluorescent ubiquitination-based cell-cycle indicator (FUCCI) (*38*) was stably expressed in a

representative luminal A subtype cell line (MCF-7) to observe real-time changes in the cell cycle (Fig. 1A). Then, we analyzed the distribution of each cell-cycle phase in the presence or absence of HRG for up to 72 h (Fig. 1B–D). Relative to that in the control, after HRG stimulation, the proportion of cells in the S/G2/M phase started to increase significantly after 24 h, and the number of nuclei, a read-out of cell number, increased 1.4-fold after 48 h, suggesting that HRG stimulation enhanced cell proliferation. Conversely, control cells showed a gradual increase in the proportion of S/G2/M cells over time but no increase in the number of nuclei, suggesting cell-cycle arrest in the S/G2/M phase in the absence of the ligand. To further examine the transition times of each phase of the cell cycle after HRG stimulation, we performed single-cell tracking and quantified the distribution of the cell-cycle phases (Fig. 1E; Fig. S1A, B). Our results indicated that the G1/S transition occurred 19.0 ± 7.2 h after HRG stimulation, while the S/G2 and M/G1 transitions occurred at 32.5 ± 9.3 h and 39.4 ± 8.7 h, respectively (Fig. 1F). These findings suggested that most cells entered the S phase approximately 20 h after HRG stimulation, with a certain degree of intercellular variability.

CDK4 and cyclin D1 are timely expressed at the G1/S transition

We further examined the signaling dynamics that lead to cell-cycle entry following HRG stimulation (*28*, *39*). We closely assessed the activity dynamics of ErbB2, AKT, and ERK pathways, following HRG stimulation (Fig. 2A, B; Fig. S2A). The results showed that p-ErbB2 levels peaked within 30 min of HRG stimulation, rapidly decreased within 2 h, and gradually increased until the S/G2M transition point (32 h). Similarly, p-AKT and p-ERK levels peaked within 30 min, followed by a gradual decrease in p-AKT levels over approximately 12 h and a rapid reduction in p-ERK levels within 4 h. Both kinases maintained moderate phosphorylation levels until the attainment of the S/G2M transition point. c-Myc and p-c-Myc levels peaked within 2 h of HRG stimulation and then decreased to basal levels till the time the G1/S transition point was reached (20 h). Conversely, although c-Fos levels peaked within 2 h and quickly reduced to basal levels, p-c-Fos showed dynamics similar to those of p-ERK, maintaining a moderate phosphorylation level until the S/G2M transition. Following ErbB2 activation, p-AKT, p-ERK, and p-c-Fos levels were maintained for a prolonged period until the S/G2M transition, whereas p-c-Myc and c-Myc levels decreased around the time of the G1/S transition.

Next, we estimated the timing of the R point from the signaling dynamics of G1/S transition regulators (Fig. 2C, D; Fig. S2B). Cyclin D1/CDK4 activity is required for the maintenance of RB inactivation from the G1 to G2 phase. Here, cyclin D1 and CDK4 levels began to increase shortly after HRG stimulation; they peaked approximately 20 h after HRG stimulation, and then gradually decreased (Fig. 2D). p-RB (Thr^{373}) (*40*) showed a time-course pattern similar to that of cyclin D1/CDK4, whereas p-RB ($Ser^{807/811}$) showed a monotonic increase similar to that of cyclin E (Fig. S2C and D), suggesting different roles for each phosphorylation site in the regulation of G1/S transition and cyclin E expression. Conversely, E2F1 expression increased

similar to that of cyclin E and CDK2 (Fig. S2C and D) in the time frame of 12–20 h after HRG stimulation. Therefore, our results suggest that cyclin D1/CDK4 may play a role in the maintenance of RB phosphorylation near the R point, which is critical for the initial step in advancing toward the G1/S transition.

A population subset undergoes cell cycle even with CDK4 inhibition

Next, we investigated whether cyclin D1/CDK4 is necessary for the G1/S transition in MCF-7 cells. As the R point may be occur approximately 12–16 h after HRG stimulation (Fig. 2D), cells were treated with a CDK4i (250 nM, a concentration that inhibited approximately 50% of the HRG-induced cyclin D1 expression) 12 h after HRG stimulation (Fig. S3A and B). As ERK activates cyclin D1 expression and AKT inhibits its degradation (*41*), we used 600 nM AKT inhibitor (AKTi) and 500 nM MEK inhibitor (ERKi), which have comparable inhibitory effects on cyclin D1 expression (Fig. S3A and B), as CDK4i. We examined the proportion of cells in each cell-cycle phase at the early (32 h) and late (72 h) time points after HRG stimulation (Fig. 3A and B). At early time points, fewer cells treated with CDK4i, AKTi, or MEKi were in the S/G2/M phase relative to non-treated cells. However, at later time points, although AKTi and MEKi reduced the proportion of cells in the S/G2/M phase, the effect of CDK4i was not observed. Additionally, the number of nuclei was significantly reduced by AKTi and MEKi after 72 h but not by CDK4i (Fig. 3C), suggesting that only AKTi and MEKi could induce cell-cycle arrest and growth inhibition in most cell populations. Furthermore, although CDK4i resulted in a cell-cycle arrest in most cells, a small number of cells did not respond to CDK4i and continued to progress, suggesting that additional mechanisms maintained the functionality of the cell cycle after CDK4i treatment.

If a phase-specific regulatory mechanism exists, it could be expected that the cell-cycle progression during CDK4 inhibition would demonstrate a different correlation between the G1/S and M/G1 phases compared to that observed with the AKTi, MEKi, and control conditions. Therefore, we compared the correlation coefficient, slope, and intercept of the regression equation of the G1/S and M/G1 phases for each inhibitor-treated cell group for up to 72 h and analyzed the timing and duration of the cell-cycle phases under conditions of inhibitor treatments (Fig. 3D; Fig. S3C). Pearson's correlation coefficients were lower for CDK4i (0.76) than for AKTi (0.91), MEKi (0.95), and control conditions (0.84). Furthermore, the slope (s) and intercept (i) of the regression equation also exhibited a lower slope ($s = 0.56$) and higher intercept ($i = 37$) in the CDK4i condition than in the AKTi (s = 1.0, i = 19), MEKi (s = 0.95, i = 17), and control conditions (s = 1.0, i = 17). These findings imply that the duration of the S/G2/M phase may not be constant in the CDK4i condition (compared to other conditions). Therefore, the correlation coefficients between the time to G1/S transition, the time to M/G1 transition, and the duration of the S/G2/M phase were examined. The CDK4i condition showed higher correlation coefficients than the other conditions (Fig. 3E). Then, we divided the

population based on their timeliness in relation to the median time of the G1/S transition, distinguishing between individuals who were early and who were late. Subsequently, we compared the duration of each S, G2, and M phase. Results revealed that the mean duration in the CDK4i treatment significantly differed between early (22.3 ± 7.2) and the late (15.8 ± 2.4), with a difference of approximately 6.5 h (Fig. S3C). However, in other conditions, no significant differences were observed between early and late. The average time for G1/S transition was longer in the CDK4i treatment (49.5 ± 13.2) than in control (24.7 ± 5.7), AKTi (39.6 ± 14.8), and MEKi (26.6 ± 11.5) conditions (Fig. 3E). Thus, the majority of CDK4i-unresponsive cells showed a clear trend toward a longer G1/S transition and a shorter S/G2/M-phase duration. These results suggest that an additional mechanism related to the control of the timing and duration of the cell-cycle transition, which was not observed in control, AKTi, and MEKi conditions, underlies the non-responsiveness of cells to CDK4 inhibition.

CDK4i enhances c-Myc transcriptional activity via H3K27Ac modification

The regulatory mechanism of gene expression may differ under CDK4i conditions as they did not exhibit a constant cell-cycle period compared to other conditions (Fig. 4A). Transcriptome and epigenetic analyses were conducted to investigate the mechanisms responsible for cell-cycle regulation post-CDK4 inhibition. To elucidate gene expression patterns during inhibitor treatment, time-course mRNA expression (control, 2, 4, 8, 12, 16, 20, 24, and 28 h after HRG stimulation), H3K27Ac and H3K4me1 modification (control, 16, 20, 24, and 28 h after HRG stimulation) were analyzed in the presence or absence of CDK4i. First, active transcription factors were predicted based on the RNA-seq data at each time point using DoRothEA (Fig. S4A). mRNAs corresponding to transcription factors, such as *Myc*, AP-1 family (*Jun*, *Fos*), *EGR1*, *NFKB1*, and *STAT3*, which are known to promote cell-cycle progression were highly enriched 4 h after CDK4i treatment (16 h after HRG stimulation). Next, motif enrichment analysis was performed to examine whether the activation of these transcription factor mRNAs was associated with promoter regions, defined as the regions in the H3K27Ac peak that did not overlap with the H3K4me1 peak (Fig. S4B and C), revealing that E-box sequences (CANNTG) (*42*) were enriched in the promoter regions at all time points following CDK4i treatment (Fig. 4B). As c-Myc is known to bind E-box sequences (*43*), c-Myc was focused on to determine its involvement in G1/S transition under conditions of CDK4 inhibition. Near the restriction point (12–16 h after HRG stimulation) of inhibitor-non-treated cells, the expression of c-Myc and p-c-Myc (Ser^{62}) decreased (Fig 1I and J), and gene set enrichment analysis (GSEA) showing normalized enrichment scores (NES) (*44*) failed to show any enrichment of Myc-target genes (n = 58, NES = -0.8963, P = 0. 6763; Fig. 4C). Nonetheless, 4 h after treatment (16 h after HRG stimulation) in the CDK4i-treatment group, Myc-target genes (n = 58, NES = 1.39358, P = 0.03597) were significantly enriched compared to that in the untreated cells (Fig. 4D). However, no significant difference was observed between the CDK4i and control conditions at subsequent time points (20, 24, and 28 h after HRG stimulation; 20 h: NES = 0.8508581, P = 0.7883; 24 h:

NES = -0.9007113, P = 0.6327; 28 h: NES = -1.180552, P = 0.2277). As c-Myc-target genes encompass a range of genes (beyond those related to the cell cycle), it would be challenging to discern significant differences when analyzing all of them collectively. Consequently, we conducted the examination of the temporal expression patterns of individual cell cycle–related genes within the c-Myc-target gene set. Specifically, we focused on genes whose promoter region exhibited a higher abundance of H3K27Ac modification compared to the enhancer region (Fig. S4D). According to the results, *CCNE1* showed substantial overexpression 16 h after HRG stimulation in the presence of CDK4i, whereas the expression of *CCND1*, *CDK1*, *CDC25A*, *E2F2*, *E2F3*, and *CDKN1B* was sustained for an extended period (20–28 h after HRG stimulation). These findings suggest that CDK4 inhibition alters the H3K27Ac levels in the promoter regions of c-Myc-target genes, leading to sustained expression of cell cycle–related genes. Therefore, the G1/S transition, originally regulated by cyclin D1-CDK4, is inhibited by CDK4i but is maintained through an alternative pathway facilitated by the transcriptional activity of c-Myc.

Next, to further explore whether the mechanism underlying the delayed G1/S transition following CDK4i treatment was due to the activation of c-Myc transcriptional activity, we tested the effects of an inhibitor of c-Myc transcriptional activity (EN4). The combination of CDK4i and EN4 resulted in a dose-dependent increase in the proportion of cells in the G1 phase and reduced number of cells in the S/G2/M phase (Fig. 4E and G), whereas no change was observed when using EN4 alone (Fig. 4H and J). These results suggest that the transcriptional activity of c-Myc is responsible for the delayed G1/S entry. To further validate these findings using clinical data, microarray data from patients with luminal A subtype of breast cancer who received long-term (16 weeks, n = 23) or short-term (4 weeks, n = 26) CDK4/6i therapy were retrospectively analyzed (*45*). *PCNA*, a Myc-target gene involved in DNA replication during G1/S transition, showed a $\log_2$ fold change (FC; long/short) of 0.5 (adj. P-value = 0.000132; Fig. 4K). Consistent with our mRNA expression data, *PCNA* expression increased after CDK4i treatment from 4 to 12 h (16 to 24 h after HRG stimulation) relative to the control (Fig. 4L). Taken together, these data suggest that CDK4 inhibition–induced epigenetic modifications activate c-Myc-target genes, ultimately contributing to cell-cycle maintenance.

CDK4i induces ErbB2 degradation and delays G1/S transition

c-Myc is known to promote G1/S transition and cell proliferation (*32*, *35*). Therefore, if the activity of c-Myc is enhanced by CDK4i, the time to G1/S transition should not be extended. As our results showed that the G1/S transition time was prolonged in CDK4i non-responders (Fig. 3E), we examined whether c-Myc expression was decreased after CDK4i treatment (Fig. 5A and B). Results showed that c-Myc expression was slightly reduced, although the difference was not statistically significant (relative to untreated cells). The levels of phosphorylated ErbB2, ERK, and AKT, which induce c-Myc mRNA expression and stabilize c-Myc protein, also decreased

after CDK4 inhibition (Fig. 5A and B). These data suggest that the CDK4i-induced downregulation of the ErbB2 pathway may result in extended G1/S transition time in wild-type (WT) MCF-7 cells.

To investigate the mechanism responsible for the CDK4i-mediated downregulation of the ErbB2 pathway, we focused on the Hsp90-chaperone system, particularly with respect to the stability and maturation of nascent ErbB2. Of note, ATP-competitive kinase inhibitors prevent ErbB2 from accessing the Hsp90-CDC37 complex, leading to its degradation (*46*). As CDK4i is an ATP-competitive kinase inhibitor, we examined the co-localization of Hsp90 and ErbB2 through immunostaining and investigated whether the CDK4i-induced downregulation of the ErbB2 pathway was attributable to a reduced interaction between ErbB2 and Hsp90 (Fig. S5A). We also quantified the co-localization of Hsp90 and PY100 to estimate the phosphorylation levels of ErbB receptors. As WT MCF-7 cells naturally express low levels of ErbB2, we used MCF-7 cells overexpressing moderate levels of ErbB2 (Fig. S5S and T). After confirming the unaltered expression of ErbB2, PY100, and Hsp90 (Fig. S5B, C, G, H), we examined the co-localization patterns using Mander's coefficient. Compared to control conditions, CDK4i treatment conditions were associated with reduced co-localization of Hsp90 with ErbB2 or PY100 (Fig. S5D, E, I, J). No significant difference was observed in the total number of nuclei in any of the images (Fig. S5F and K). These results suggest that CDK4i inhibited the interaction between Hsp90 and ErbB2, leading to ErbB2 misfolding. As reported previously, ErbB2 expression was reduced 8 h after CDK4i treatment (20 h after HRG stimulation); however, the levels of ErbB2 mRNA did not change regardless of CDK4i treatment (Fig. S5L and M). Thus, we hypothesized that the downregulation of ErbB2 may be due to its protein degradation. We tested this hypothesis using the proteasome inhibitor MG132. Our results showed that, upon MG132 treatment, ErbB2 expression was not reduced relative to the control condition (Fig. S5N–P). These findings suggested that CDK4i disrupts the interaction between Hsp90 and ErbB2, thereby triggering ErbB2 degradation. Further, when we used the Hsp90 inhibitor geldanamycin (GA) at a concentration that effectively suppressed ErbB2 expression by 40%, comparable to the inhibitory effect of CDK4i (Fig. S5O and P), cell-cycle progression was almost entirely halted without a significant delay in the G1/S transition (Fig. S5Q, R; Movie 1). Taken together, the timing of the G1/S transition is primarily regulated by the activation of the ErbB2 signaling pathway under the condition of Hsp90-mediated ErbB2 stabilization. The stability of ErbB2 may play a crucial role in the regulation of the c-Myc-mediated G1/S transition, specifically when the transition is modulated through epigenetic alterations triggered by CDK4i.

ErbB2 expression induces cell-cycle arrest after CDK4 inhibition

To test the hypothesis that ErbB2 overexpression neutralizes the delayed G1/S entry observed in WT MCF-7 cells, we established MCF-7 cells that expressed varying levels of ErbB2, ranging from moderate to high (Fig. S5S and T), and analyzed the cell-cycle distribution using live

imaging (Fig. 5C). In cells expressing high levels of ErbB2, the proportion of cells in the S/G2/M phase was considerably reduced following CDK4i treatment, whereas the percentage of cells in the G1 phase was significantly increased (Fig. 5D). This indicates that the cell cycle was arrested after CDK4i treatment in most cells expressing high levels of ErbB2. However, a few non-responders exhibited a decreased G1/S transition time and shorter duration of the S/G2/M phases in inhibitor-treated conditions (compared to control conditions), with the extent of these effects being dependent on ErbB2 expression (Fig. 5E and F). Thus, in CDK4i non-responders, ErbB2 overexpression suppressed the overall cell-cycle delay observed in WT cells.

Next, to unveil the mechanism underlying the cell-cycle arrest observed in the majority of CDK4i-treated ErbB2-overexpressing cells, we examined the expression of cyclin D1, which plays a pivotal role in the determination of cell-cycle progression or arrest (*1*). The results indicated significantly reduced cyclin D1 expression and p-RB levels in cells expressing high ErbB2 levels after CDK4i treatment relative to other conditions (Fig. 5A and B). Thus, we investigated the cause behind the decreased cyclin D1 levels after CDK4i treatment in ErbB2-overexpressing cells. p27 is known to facilitate the assembly of cyclin D1/CDK4 complex; conversely, p27 expression is inhibited by p-AKT and c-Myc. Our data showed that p27 expression was reduced after CDK4i treatment in ErbB2-overexpressing cells, whereas p-AKT and c-Myc expression tended to increase after inhibitor treatment. However, p-ERK levels did not differ between different conditions, suggesting that in ErbB2-overexpressing cells, the expression of p27 and cyclin D1 is suppressed by the activation of the p-AKT–c-Myc axis after CDK4 inhibition, thereby leading to cell-cycle arrest in most cells. In particular, according to single-cell data obtained in the condition without CDK4i, we observed that the G1/S transition time was delayed by approximately 2–3 h in high ErbB2-expressing cells (OE-High, 25.2 ± 6.6 h) compared to control (23.3 ± 5.2 h) and cells expressing moderately high levels of ErbB2 (OE-Moderate, 22.2 ± 4.7 h; Fig. 5E). Further, the slope (s) and intercept (i) values showing the correlation between the G1/S and M/G1 transitions also increased depending on ErbB2 expression (Control: $s = 0.83$, $i = 19$; OE-Moderate: $s = 1.2$, $i = 22$; OE-High: $s = 0.88$, $i = 30$). Overall, our findings suggest that cyclin D1 expression tends to decrease due to the suppression of p27 via activation of the AKT–c-Myc axis in ErbB2 overexpressing cells, ultimately prolonging each cell-cycle phase compared to that in control cells, as also evidenced by the number of nuclei observed in each phase (Fig. 5G). Based on these observations, we propose that following CDK4 inhibition, the transcriptional activity of c-Myc increases in cells expressing high ErbB2 levels, a scenario that further facilitates the repression of cyclin D1 expression.

Reversible cell-cycle arrest is sustained by c-Myc transcriptional activity

Drug resistance is closely linked to reversible cell-cycle arrest (*11*). Therefore, to investigate whether the cell-cycle arrest observed after CDK4i treatment in cells with high ErbB2 levels was reversible, the expression of proteins regulating the G1/S transition and the percentage of cells

undergoing the G1/S transition were examined following CDK4i washout. The results showed that the levels of cyclin D1, p27, and p-RB increased after CDK4i washout (compared to the control condition); however, c-Myc expression remained unchanged (Fig. 6A and B). Thus, c-Myc phosphorylation (Ser^{62}) was further validated at the single-cell level to confirm the elevated transcriptional activity of c-Myc in cell cycle–arrested cells. We also quantified the phosphorylated c-Myc (Ser^{62}) to phosphorylated cyclin D1 (p-c-Myc/cyclin D1) ratio at the single-cell level and the percentage of cells in the S/G2/M phase, based on changes in DAPI staining (Fig. 6C). Histograms showed that the p-c-Myc/cyclin D1 ratio was lower following CDK4i washed out compared to the control condition. In particular, the percentage of cells in the S phase increased from 18.7% to 47.5% after washing out CDK4i. In addition, the p-c-Myc/cyclin D1 ratio was maintained in ErbB2-overexpressing cells compared to control cells (Fig. S6A). These findings imply that sustained cell-cycle arrest in ErbB2-overexpressing cells may be attributed to the sustained transcriptional activation of c-Myc. Furthermore, we investigated whether the inhibition of c-Myc transcriptional activity prevented reversible cell-cycle arrest. After treatment with or without EN4 and CDK4i for 8 h and subsequent washing, the ratio of cells in the G1 phase to those in the S/G2/M phase was examined at 52 h (72 h after HRG stimulation; Fig. 6D and E). Notably, the combination of EN4 and CDK4i reduced the percentage of cells in the S/G2/M phase and increased the percentage of cells in the G1 phase, suggesting the impairment of cell-cycle reentry. Further, although the levels of p27 (*CDKN1B*) mRNA were reduced by CDK4i treatment compared to that in the control condition over time, the combination of EN4 and CDK4i rescued the p27 mRNA levels (Fig. 6F and G). This suggested that p27 mRNA levels were directly reduced via c-Myc transcriptional activity following CDK4i treatment. Overall, these data support the hypothesis that in cells expressing high levels of ErbB2, CDK4 inhibition leads to reversible cell-cycle arrest via an excessive increase in c-Myc transcriptional activity and a rapid decrease in cyclin D1 levels through the reduction of p27 mRNA levels. Altogether, ErbB2 expression patterns determine the c-Myc to cyclin D1 ratio in the G1/S regulatory network, resulting in dynamic changes in sensitivity to CDK4is.

DISCUSSION

In this study, we primarily focused on the ErbB2-mediated mechanisms of G1/S entry in breast cancer cells. An ErbB2-overexpressing subpopulation has been observed among luminal A breast cancer cells, which were initially characterized by low ErbB2 expression (*24*). Given the relatively infrequent occurrence of such cell subpopulations, at around 7% (*47*), identifying differences in the cell-cycle transition during the initial step of cell proliferation, with a focus on ErbB2 expression, is crucial to effectively combating cancer. Long-term CDK4i treatment, commonly used for luminal A breast cancer, triggers the activation of alternative pathways such as PI3K/AKT/mTOR signaling, Androgen receptor signaling, and Hippo signaling (*13*, *14*, *18*–

20), as well as transcriptional reprogramming via non-coding RNAs (*21*, *48*), gradually leading to the emergence of drug resistance. In particular, prolonged administration of drugs can lead to drug resistance through the persistence of survival signals and activation of alternative signaling pathways. Therefore, to curtail drug resistance, it is imperative to inhibit potential survival signals that may act at very early stages by identifying and inhibiting specific cell-cycle entry pathways. To this end, we elucidated how the differences in ErbB2 expression patterns within the same luminal A breast cancer cell population might alter the cell-cycle regulatory network and cell sensitivity to CDK4is (Fig. 7A and B).

In this study, we analyzed the temporal dynamics of the cell cycle using time-course data to elucidate how the expression and activation patterns of cyclin D1 and c-Myc, which are crucial regulators of the G1/S transition, vary depending on the expression status of ErbB2, ultimately affecting the time to G1/S entry and the duration of cell-cycle phases. In MCF-7 cells, a representative luminal A breast cancer cell line with low ErbB2 expression, the G1/S transition was shown to be regulated by the cyclin D1/CDK4 complex via Hsp90, under stable ErbB2 expression conditions. CDK4 inhibition tended to induce cell-cycle arrest in several cell types, whereas the G1/S transition time was delayed due to epigenetic modification of c-Myc transcriptional activity in a subpopulation of CDK4i non-responders. Furthermore, the AKT and c-Myc pathways were more active in MCF-7 cells expressing high levels of ErbB2 than in WT cells, indicating that c-Myc is more heavily involved in regulating the G1/S transition. Therefore, it was suggested that the excessive transcriptional activity of c-Myc induced by CDK4 inhibition paradoxically led to reversible cell-cycle arrest by rapidly reducing cyclin D1 levels via the suppression of p27 expression. ErbB2 and ErbB3 heterodimers have been reported as potent activators of the AKT/PI3K pathway (*49*, *50*), and the activation of the AKT and c-Myc pathways observed in MCF-7 cells expressing high ErbB2 levels indicates that more ErbB2 and ErbB3 heterodimers are formed upon HRG stimulation than in WT cells. Furthermore, the expression of p27, which recruits cyclin D1 to the nucleus during the G1 phase, is repressed by AKT and c-Myc (*35*). Therefore, in high ErbB2-expressing MCF-7 cells, CDK4 inhibition further increases the levels of free cyclin D1, which is more prone to degradation, causing a hypophosphorylated state of RB and leading to cell-cycle arrest (*51*–*53*). Conversely, c-Myc regulates two opposing cell fate mechanisms, i.e., the cell survival pathway (cell-cycle progression) and the apoptotic pathway (*32*, *35*, *54*). In ErbB2-overexpressing MCF-7 cells, cell-cycle arrest was reversible after CDK4 inhibition, suggesting that the transcriptional activity of c-Myc observed in this study sustained cell survival. Taken together, these results suggest that the co-treatment with inhibitors targeting the transcriptional activity of c-Myc is necessary to impose the irreversible the cell-cycle arrest caused by CDK4 inhibition. Nonetheless, for future considerations of drug responses, a more comprehensive analysis, including single-cell multi-omics analysis, is warranted to determine the threshold at which c-Myc induces cell survival or apoptosis. Finding the threshold levels at which c-Myc no longer supports survival and induces

cell death in terms of ErbB2 expression levels could then lead to better drug treatment plans for breast cancer.

In summary, in this study, we revealed the effect of different ErbB2 expression patterns on cell-cycle regulation in luminal A breast cancer cells. Additionally, we demonstrated the potential of CDK4i to delay cell-cycle progression through epigenetic modifications mediated by c-Myc. Low ErbB2 expression sustained c-Myc activity for gradual cell-cycle progression. Conversely, high ErbB2 expression led to increased c-Myc transcriptional activity and induced cell-cycle arrest. However, considering the functional survival signals facilitated by c-Myc activity, this proposes a problematic scenario in which apparently halted proliferation in subpopulations exhibiting high ErbB2 expression presents an opportunity for resumed proliferation. Our results suggest that assessing the c-Myc to cyclin D1 ratio could provide a quantitative understanding of the varied sensitivity to CDK4is, influenced by differing ErbB2 expression patterns, while avoiding misinterpretation based solely on the observable cell proliferation rate.

Acknowledgments:

We thank all members of the Laboratory for Cell Systems at the Institute for Protein Research for discussing this research, and especially Mr. Kyoichi Ebata for helping to develop the cell-cycle analysis. We also thank Mr. Hideya Aragaki from Olympus Corporation for providing the cell-tracking software.

Funding:

JSPS KAKENHI (18H04031, MO; 21K15503, ANI)

JST CREST Program (JPMJCR21N3, MO)

Uehara Memorial Foundation (MO)

Kaneko Narita Research Grant from the Protein Research Foundation (ANI)

New Field Development Support Program from Institute for Protein Research (ANI)

Joint Research Grant from ExCELLS (MO, KA)

Author contributions:

Conceptualization: ANI, MO
Methodology: ANI, KM, KA, MO
Validation: ANI
Formal analysis: ANI, KM
Investigation: ANI, KM
Resources: ANI, KA, MO
Visualization: ANI, KM
Writing – Original Draft: ANI, KM, MO
Writing – Review & Editing: ANI, KM, KA, MO
Supervision: ANI, MO
Project administration: ANI, MO
Funding acquisition: ANI, KA, MO

Competing interests: Authors declare that they have no competing interests.

MATERIALS AND METHODS

Reagents

PD0325901, the MEKi, was purchased from FUJIFILM Wako Pure Chemical Corp. (Osaka, Japan); CDK4i V was procured from Calbiochem (CA, USA); AKTi VIII was procured from Cayman Chemical (Ann Arbor, MI, USA); blasticidin was purchased from Kaken Pharmaceutical (Tokyo, Japan); puromycin was obtained from Santa Cruz Biotechnology (Santa Cruz, CA, USA); Lipofectamine LTX was purchased from Thermo Fisher Scientific (Thermo Fisher Scientific); HRG was procured from R&D Systems, Inc (MN, USA).

ErbB2 overexpression

A method for constructing MCF-7 (ATCC, HTB-22) overexpressing full-length human ErbB2 (HER2) is described as follows: A human ErbB2 cDNA in pCMV6-XL5 vector was purchased from OriGene (Catalog No: TC128161, Rockville, MD). The cDNA fragment was cloned into the vector pCMV-6-Neo vector (OriGene). The plasmid was then transfected into MCF-7 cells using the Lipofectamine LTX (Invitrogen, Carlsbad, CA) according to the manufacturer's protocol, and stable transfectants were selected with G418 (neomycin). Colonies derived from single cells compartmentalized in 96-well plates were isolated and examined the ErbB2 expression level was examined to obtain cells expressing the moderate or high ErbB2 by western blotting as described below (protein extraction and immunoblotting).

Cell culture

MCF-7 and ErbB2-overexpressing MCF-7 cells were cultured in Dulbecco's modified Eagle's medium (Nakalai Tesque, Kyoto, Japan) supplemented with 10% (v/v) fetal bovine serum (FBS, Sigma-Aldrich) and 1% penicillin-streptomycin (100 IU/mL penicillin, 100 μg/mL streptomycin; Nacalai Tesque, Kyoto, Japan) at 37 °C in a humidified 5% CO_2 atmosphere. MCF-7 and ErbB2-overexpressing MCF-7 cells were routinely tested using the CycleavePCR Mycoplasma Detection Kit (Takara bio, CY-232). None of the cell lines were contaminated with mycoplasma.

FUCCI transfection

MCF-7 cells and HER2-overexpressed MCF-7 cells stably expressing the FUCCI biosensor were generated using the PiggyBac transposase system (*55*). Lipofectamine LTX (Thermo Fisher Scientific, USA) was used to transfect FUCCI plasmid (pPBbsr2-H2B-iRFP-P2A-mScarlet-I-hGem-P2A-PIP-tag-NLS-mNeonGreen; https://benchling.com/s/seq-LPZ1tLdpgnpJIYOG2ujR) along with hyPBase (https://benchling.com/s/seq-oGkw53b41IZqvzF5yQ9K) into MCF-7 and HER2-overexpressing MCF-7 cells, as per following manufacturer's protocol (*56*). For separating cells that stably expressed the plasmid, cells were suspended in drug-free medium for 48 h, followed by blasticidin treatment (10 μg/mL). Colonies derived from single cells compartmentalized in 96-well plates were selected by microscopic live-cell observation, which showed Geminin and PIP-tag fluorescence.

Nuclei count

The number of nuclei was quantified based on the fluorescence of the FUCCI probes, and a nuclear marker (histone H2B), mScarlet-hGem and PIP-tag-mNeonGreen signals were used as an indicator of cell proliferation. Image processing and quantification of the nuclear ratio were performed using ImageJ-Fiji software (version 1.53, NIH). Masks of the merged nuclear marker, mScarlet-hGem and PIP-tag-mNeonGreen signals were obtained by applying a fixed threshold. The obtained masks were identified using 'Analyze Particles' and automatically counted as regions of interest (ROIs). The nuclear ratio was calculated by dividing the number of nuclei at the end of the imaging by the number of nuclei at the beginning. Thus, the nuclear ratio indicated potential cell-cycle arrest if it was close to 1.0, cell proliferation if it exceeded 1.0, and apoptosis if it was less than 1.0.

Protein extraction and immunoblotting

Total cell lysates were prepared in RIPA buffer (Nakalai Tesque, 1648834) containing protease inhibitors (Roche, 11836153001) and phosphatase inhibitors (Roche, 4906837001) at 4 °C. Cells were vortexed for 5 min, centrifuged at 16, 000 x g for 15 min at 4 °C, and the supernatant was collected. The supernatant was denatured by heating at 95 °C with sample buffer (5×) and 2-mercaptoethanol (Nakalai Tesque, 21418-55) for 5 min. SDS polyacrylamide gel electrophoresis (Nacalai Tesque, 1306644) was performed, and the proteins were transferred to polyvinylidene fluoride membranes (Merck, Germany) and incubated with 10% blocking buffer (Nacalai Tesque, 03953-95) prepared in Tris-buffered saline/Tween 20 (Takara Bio, T9142) (TBS-T) for 1 h at 25 °C. Membranes were probed overnight with antibodies against AKT (1:1000; Cell Signaling Technology; #4685), p-AKT (Thr^{308}; 1:1000; Cell Signaling Technology; #2965), ERK (1:1000; Cell Signaling Technology; #9102), p-ERK (Thr^{202} Tyr^{204}; 1:1000; Cell Signaling Technology; #4370), HER2/ErbB2 (1:1000; Cell Signaling Technology; #2165), p-HER2/ErbB2 ($Thr^{1221/1222}$; 1:1000; Cell Signaling Technology; #2249), p-c-Fos (Ser^{374}; 1:1000; Abcam; #ab55836), c-Fos (1:200; Santa Cruz; #sc-166940), p-c-Myc (Ser^{62}; 1:1000; Abcam; #ab51156), c-Myc (1:200; Santa Cruz; #sc-40), E2F-1 (1:1000; Cell Signaling Technology; #3742), p-RB ($Ser^{807/811}$; 1:1000; Cell Signaling Technology; #8516), p-RB (Thr^{373}; 1:1000; Abcam; #ab52975), RB1 (1:1000; NOVUS biologicals; #SPM353), cyclin D1 (1:1000; Cell Signaling Technology; #2978), cyclin E (1:200; Santa Cruz; #sc-247), cyclin A (1:200; Santa Cruz; #sc-271682), CDK4 (1:1000; Santa Cruz; #DSC-35), CDK2 (1:1000; Santa Cruz; #D-12), P27 Kip1 (1:1000; Cell Signaling Technology; #3686), and GAPDH (1:4000; Proteintech, MA, USA; 10494-1-AP) in TBS-T including 10% blocking buffer at 4 °C. They were then incubated with horseradish peroxidase (HRP)-conjugated secondary antibodies [HRP-conjugated anti-mouse IgG (1:5000; Cell Signaling Technology; #7076) and HRP-conjugated anti-rabbit IgG (1:5000; Cell Signaling Technology; #7074) for 1 h at room temperature. The membranes were developed using a chemiluminescent HRP substrate (Merck, Germany). Protein bands were detected using an Amersham Imager 600 UV (GE Healthcare, Eindhoven, Netherlands) and visualized using

ImageJ-Fiji software (version 1.53t, NIH).

qRT-PCR

RNA was isolated from cells using NucleoSpin RNA Plus (Macherey-Nagel, Duren, Germany, Cat. No. 740984.250) according to the manufacturer's protocol. cDNA was synthesized using the ReverTra Ace qPCR RT Master Mix (TOYOBO, Osaka, Japan), and quantitative PCR was performed using a KOD SYBR qPCR kit (TOYOBO) on a CFX96 Real-Time PCR System (Bio-Rad Laboratories, Hercules, CA, USA). PCR conditions were as follows: 95°C for 30 sec, followed by a maximum of 40 cycles of 98°C for 5 sec, and 60°C for 30 sec. The ΔΔCq method was used to quantify gene expression, using RPL27 expression as an internal reference (*57*). The primers used for real-time PCR are listed in Supplementary Table 1.

Live-cell imaging and image quantification

Time-lapse microscopy images were acquired using an IN Cell Analyzer 2500HS (GE Healthcare Life Science) equipped with a CFI S Plan Fluor ELWD dry objective lens 20× (NA: 0.45) using an excitation wavelength of 475 nm and an emission wavelength of 511 nm for PIP-tag-mNeonGreen, and an excitation wavelength of 542 nm and an emission wavelength of 597 nm for mScarlet-hGem. Cells were maintained at 37 °C in a humidified 5% CO_2 atmosphere and imaged at 20-minute intervals for 60 h. Image processing and quantification of the percentage of cells in each cell-cycle phase were performed using ImageJ-Fiji software (version 1.53, NIH). Masks of the mScarlet-hGem and PIP-tag-mNeonGreen signals were obtained by applying a fixed threshold. The obtained masks were identified using 'Analyze Particles' and automatically counted as regions of interest (ROIs). Cell-cycle phases were determined in the following manner: G1 phase, PIP-tag-positive; S phase, hGem-positive; G2/M phase, PIP-tag- and hGem-positive. The average brightness of mScarlet and mNeonGreen was obtained using cell-tracking software (Olympus). The threshold parameters for mScarlet and mNeonGreen for each cell were set manually. Subsequently, an algorithm for estimating the cell-cycle phase assembled using R packages [brunnermunzel (v.1.4.1), multimode (v.1.4), rlist (v.0.4.6.1), and tidyverse (v.1.3.0)] was employed to determine the cell-cycle phase at the single-cell level. The duration of each cell cycle phase was obtained from the single-cell data.

Immunostaining

MCF-7 cells and cells overexpressing ErbB2 (moderate or high) were seeded in 12-well plates at a density of 200,000 cells per well and cultured in 10% FBS containing DMEM for 48 hours. The medium was then changed to FBS-free phenol red-free DMEM (FUJIFILM Wako Pure Chemical Corp.) and the cells were cultured for 17 h, then the medium was changed again and the cells were cultured for 3 h. After administration of 10 nM HRG (R&D Systems, Inc.) for 12 h, the cells were independently treated with CDK4i and DMSO. Cells were washed twice with PBS at the indicated times and fixed for 2 min with pre-prepared methanol at -20 °C. They were then washed twice with Blocking One (Nacalai Tesque, 03953-95) and incubated overnight at

4 °C with primary antibodies diluted in 10% goat serum (Thermo Fisher Scientific, 16210064)/Blocking One. Following this, cells were washed five times with PBS and incubated with fluorescent dye–conjugated secondary antibody, 2 μg·mL^{-1} DAPI (Nacalai Tesque, 11034-56), and 0.5 μg·mL^{-1} CellMask™ (Thermo Fisher Scientific, H32721) for 1 h at room temperature. Cells were then washed five times with PBS, and images were acquired using an IN Cell Analyzer 2500HS (GE Healthcare Life Science, USA) at 20× magnification. At least three images from each experimental condition, containing at least 100 cells, were used for quantification.

RNA-seq

FUCCI-expressing MCF-7 cells were seeded in 6-well plates at a density of 450,000 cells per well and cultured in 10% FBS containing DMEM for 48 hours. The medium was then changed to FBS-free phenol red-free DMEM and the cells were cultured for 17 h, then the medium was changed again and the cells were cultured for 3 h. After administration of 10 nM HRG for 12 h, the cells were independently treated with CDK4i and DMSO. Cells were washed twice with PBS at the indicated times. Total RNA was isolated using NucleoSpin RNA Plus (Macherey-Nagel, Duren, Germany, Cat. No. 740984.250) at the respective specified time. Library construction and RNA-seq were performed on an Illumina sequencing platform (Rhelixa). Poly(A) RNA was prepared with the Poly(A) mRNA Magnetic Isolation Module (New England Biolabs, E7490), and the sequencing library was generated using the NEBNext® Ultra™II Directional RNA Library Prep Kit (New England Biolabs, E7760). RNA-seq was performed on NovaSeq 6000 (Illumina, USA) with 150-base pair (bp) paired-end reads. Raw reads were quality-checked using FastQC (version 0.11.9) and trimmed using TrimGalore (version 0.6.0) (*58*). Trimmed reads were mapped using STAR (version 2.7.9a) (*59*) with GRCh38 as the reference genome. featureCounts (version 1.6.4) (*60*) was used to construct the count matrix with parameters as "-p -B -t exon -g gene_name." Raw counts were converted to Transcripts Per Kilobase Million (TPM) and corrected using EdgeR (version 3.36.0) (*61*). Principal components analysis (PCA) was performed using the prcomp() function in R (version 4.1.1) (*62*). GSEA was performed using the fgsea package (version 1.20.0) (*63*) and the hallmark gene set in the Human MSigDB Collections (*44*).

ChIP-seq

FUCCI-expressing MCF-7 cells were seeded in 100 mm dishes at a density of 2,300,000 cells per dish and cultured in 10% FBS containing DMEM for 48 hours. The medium was then changed to FBS-free phenol red-free DMEM and the cells were cultured for 17 h, then the medium was changed again and the cells were cultured for 3 h. After administration of 10 nM HRG for 12 h, the cells were independently treated with CDK4i and DMSO. Cells were washed twice with PBS at the indicated times. Cells were fixed with 1% formaldehyde (Thermo Fisher Scientific) for 5 min. Fragmented DNA was obtained using a SimpleChIP(R) Plus Enzymatic Chromatin IP (CST, 9005) kit and an M220-focused ultrasonicator (Covaris).

Immunoprecipitated DNA was obtained using the Auto iDeal ChIP-seq kit for Histones ×24 (Diagenode) on the SX-8G platform (Diagenode). Next, 2 µg anti-H3K27Ac antibody (Diagenode) and 2 µg anti-H3K4me1 antibody (Diagenode) were mixed with 10 µL DiaMag Protein A-coated magnetic beads, and IP reactions with DNA were performed for 12 h. De-crosslinking was conducted using 4 µl of 5 M NaCl and 1 µl of 20 mg/ml proteinase K (Thermo Fisher Scientific) for 4 h at 60 °C. Library construction and RNA-seq were performed using an Illumina sequencing platform (Rhelixa). A sequencing library was generated using the NEBNext Ultra II DNA Library Prep Kit for Illumina (New England Biolabs, 7645). ChIP-seq was carried out on NovaSeq 6000 (Illumina, USA) with 150-base pair (bp) paired-end reads. H3K27Ac ChIP-seq and H3K4me1 data were processed using the same protocol as for RNA-seq. FastQC (version 0.11.9) was used for quality control. Trimming was performed using Trimmomatic (version 0.39) (*64*) with the following parameters: ILLUMINACLIP, TruSeq2-SE; fa, 2:30:10; LEADING, 30; TRAILING, 30; SLIDINGWINDOW, 4:15; MINLEN, 30; HEADCROP, 2. Reads were mapped using Bowtie2 (version 2.4.4) (*65*) with GRCh38 as the reference genome, and duplicate reads were excluded using Picard (version 2.26.6) (*66*). Bigwig files were created from the generated BAM files using deepTools (version 3.5.1; bamCoverage function) (*67*). Peak regions were identified using HOMER (version 4.11) (*68*) with parameters "-style histone -L 0 -fdr 0.00005". All detected peak regions were annotated to their nearest neighbor genes using HOMER annotatePeaks.pl (version 4.11).

Promoter and enhancer detection

Promoter regions were defined as the regions in the H3K27Ac peak that did not overlap with the H3K4me1 peak and were within 250 bp of the transcription start site (TSS; at the center of the peak). Enhancer regions were defined as the regions in the H3K27Ac peak overlapping with the H3K4me1 peak and were more than 250 bp from the TSS, which was at center of the peak. The TSS was obtained from the Ensembl database using BiomaRt (version 2.50.3) (*69*). The bed files containing the promoter and enhancer regions for all time points were merged, and the time course of the coverage values of H3K27Ac ChIP-seq was calculated using HOMER annotatePeaks.pl (version 4.11). The estimated coverage values were used to detect promoters and enhancers affected by the CDK4is. Promoters that gained or lost signal due to CDK4is were defined as those with H3K27Ac ChIP-seq coverage values of $|\log_2 FC| > 0.3$ for inhibitor and control conditions. Enhancers that gained or lost signals due to CDK4is were defined as those that changed the coverage value of H3K27Ac ChIP-seq by $|\log_2 FC| > 0.3$, and target gene expression changes $|\log_2 FC| > 0.2$ in the same direction as the change in enhancer activity.

Motif analysis of ChIP-seq data

Motif analysis was performed using MEME Suite SEA (version 5.4.1) (*70*). The motif files were obtained from the JASPAR 2022 database (JASPAR2022_CORE_vertebrates_ nonredundant _v2) (*71*). Peak regions containing motifs were detected using the MEME Suite FIMO (version 5.4.1). The analysis was performed using default parameters.

Myc-target gene analysis

Target genes for Myc were determined using the DoRothEA database and were defined as those registered in the R DoRothEA library (version 1.6.0) (*72*) with “confidence” of “A” and “B” and positive control (mor = 1). Myc-target genes were clustered using $\log_2$ FC time-course data from 0 h for each gene. The distance between genes was calculated using Euclidean distance and classified into six clusters using Ward's method. The average $\log_2$ FC time course for each cluster was calculated by averaging the $\log_2$ FC of the genes in the cluster. The promoter and enhancer regions associated with each gene were defined as the promoter and enhancer regions associated with each cluster. The normalized motif ratio was determined by calculating the ratio of promoters to enhancers associated with each cluster containing a particular motif.

Clinical data

Microarray gene expression data (GEO GSE93204) from biopsy samples from the NeoPalAna clinical trial (NCT01723774) (*45*) were used, and differentially expressed genes were analyzed using *P*-values adjusted using the Benjamini–Hochberg method that is employed to control the false discovery rate in GEO2R.

Statistical analysis

Statistical analysis and data visualization was performed in R (version 4.2.1). To assess normality for the Kolmogorov-Smirnov test. If the data set followed a normal distribution, Student's t-test and Welch’s two-sample t-test after confirming equal variances using the F-test for comparisons between two groups. One-way ANOVA for more than two groups, followed by Tukey's post hoc test. If the data set did not follow a normal distribution, a Kruskal-Wallis test or Mann-Whitney U test was used. P-values < 0.05 were considered significant.

REFERENCES:

1. A. Zetterberg, O. Larsson, Kinetic analysis of regulatory events in G1 leading to proliferation or quiescence of Swiss 3T3 cells. *Proc. Natl. Acad. Sci. U. S. A.* **82**, 5365–5369 (1985).

2. S. M. Rubin, J. Sage, J. M. Skotheim, Integrating Old and New Paradigms of G1/S Control. *Mol. Cell* **80**, 183–192 (2020).

3. H. K. Matthews, C. Bertoli, R. A. M. de Bruin, Cell cycle control in cancer. *Nat. Rev. Mol. Cell Biol.* **23**, 74–88 (2022).

4. Q. Yu, Y. Geng, P. Sicinski, Specific protection against breast cancers by cyclin D1 ablation. *Nature* **411**, 1017–1021 (2001).

5. T. Adon, D. Shanmugarajan, H. Y. Kumar, CDK4/6 inhibitors: a brief overview and prospective research directions. *RSC Adv.* **11**, 29227–29246 (2021).

6. U. Asghar, A. K. Witkiewicz, N. C. Turner, E. S. Knudsen, The history and future of targeting cyclin-dependent kinases in cancer therapy. *Nat. Rev. Drug Discov.* **14**, 130–146 (2015).

7. B. Weigelt, J. L. Peterse, L. J. van ’t Veer, Breast cancer metastasis: markers and models. *Nat. Rev. Cancer* **5**, 591–602 (2005).

8. C. M. Perou, T. Sørlie, M. B. Eisen, M. van de Rijn, S. S. Jeffrey, C. A. Rees, J. R. Pollack, D. T. Ross, H. Johnsen, L. A. Akslen, O. Fluge, A. Pergamenschikov, C. Williams, S. X. Zhu, P. E. Lønning, A. L. Børresen-Dale, P. O. Brown, D. Botstein, Molecular portraits of human breast tumours. *Nature* **406**, 747–752 (2000).

9. T. Sørlie, C. M. Perou, R. Tibshirani, T. Aas, S. Geisler, H. Johnsen, T. Hastie, M. B. Eisen, M. van de Rijn, S. S. Jeffrey, T. Thorsen, H. Quist, J. C. Matese, P. O. Brown, D. Botstein, P. E. Lønning, A. L. Børresen-Dale, Gene expression patterns of breast carcinomas distinguish tumor subclasses with clinical implications. *Proc. Natl. Acad. Sci. U. S. A.* **98**, 10869–10874 (2001).

10. R. S. Finn, J. Dering, D. Conklin, O. Kalous, D. J. Cohen, A. J. Desai, C. Ginther, M. Atefi, I. Chen, C. Fowst, G. Los, D. J. Slamon, PD 0332991, a selective cyclin D kinase 4/6 inhibitor, preferentially inhibits proliferation of luminal estrogen receptor-positive human breast cancer cell lines in vitro. *Breast Cancer Res.* **11**, R77 (2009).

11. F. Lüönd, S. Tiede, G. Christofori, Breast cancer as an example of tumour heterogeneity and

tumour cell plasticity during malignant progression. *Br. J. Cancer* **125**, 164–175 (2021).

12. N. McGranahan, C. Swanton, Clonal Heterogeneity and Tumor Evolution: Past, Present, and the Future. *Cell* **168**, 613–628 (2017).

13. C. Michaloglou, C. Crafter, R. Siersbaek, O. Delpuech, J. O. Curwen, L. S. Carnevalli, A. D. Staniszewska, U. M. Polanska, A. Cheraghchi-Bashi, M. Lawson, I. Chernukhin, R. McEwen, J. S. Carroll, S. C. Cosulich, Combined Inhibition of mTOR and CDK4/6 Is Required for Optimal Blockade of E2F Function and Long-term Growth Inhibition in Estrogen Receptor–positive Breast Cancer. *Mol. Cancer Ther.* **17**, 908–920 (2018).

14. M. T. Herrera-Abreu, M. Palafox, U. Asghar, M. A. Rivas, R. J. Cutts, I. Garcia-Murillas, A. Pearson, M. Guzman, O. Rodriguez, J. Grueso, M. Bellet, J. Cortés, R. Elliott, S. Pancholi, C. J. Lord, J. Baselga, M. Dowsett, L.-A. Martin, N. C. Turner, V. Serra, Early Adaptation and Acquired Resistance to CDK4/6 Inhibition in Estrogen Receptor–Positive Breast Cancer. *Cancer Res.* **76**, 2301–2313 (2016).

15. S. Pancholi, R. Ribas, N. Simigdala, E. Schuster, J. Nikitorowicz-Buniak, A. Ressa, Q. Gao, M. F. Leal, A. Bhamra, A. Thornhill, L. Morisset, E. Montaudon, L. Sourd, M. Fitzpatrick, M. Altelaar, S. R. Johnston, E. Marangoni, M. Dowsett, L.-A. Martin, Tumour kinome re-wiring governs resistance to palbociclib in oestrogen receptor positive breast cancers, highlighting new therapeutic modalities. *Oncogene* **39**, 4781–4797 (2020).

16. A. Polk, I. L. Kolmos, I. Kümler, D. L. Nielsen, Specific CDK4/6 inhibition in breast cancer: a systematic review of current clinical evidence. *ESMO Open* **1**, e000093 (2016).

17. J. L. Dean, C. Thangavel, A. K. McClendon, C. A. Reed, E. S. Knudsen, Therapeutic CDK4/6 inhibition in breast cancer: key mechanisms of response and failure. *Oncogene* **29**, 4018–4032 (2010).

18. E. S. Knudsen, V. Kumarasamy, A. Ruiz, J. Sivinski, S. Chung, A. Grant, P. Vail, S. S. Chauhan, T. Jie, T. S. Riall, A. K. Witkiewicz, Cell cycle plasticity driven by MTOR signaling: integral resistance to CDK4/6 inhibition in patient-derived models of pancreatic cancer. *Oncogene* **38**, 3355–3370 (2019).

19. W. Ji, Y. Shi, X. Wang, W. He, L. Tang, S. Tian, H. Jiang, Y. Shu, X. Guan, Combined Androgen receptor blockade overcomes the resistance of breast cancer cells to palbociclib. *Int. J. Biol. Sci.* **15**, 522–532 (2019).

20. Z. Li, P. Razavi, Q. Li, W. Toy, B. Liu, C. Ping, W. Hsieh, F. Sanchez-Vega, D. N. Brown, A. F. Da Cruz Paula, L. Morris, P. Selenica, E. Eichenberger, R. Shen, N. Schultz, N. Rosen,

M. Scaltriti, E. Brogi, J. Baselga, J. S. Reis-Filho, S. Chandarlapaty, Loss of the FAT1 Tumor Suppressor Promotes Resistance to CDK4/6 Inhibitors via the Hippo Pathway. *Cancer Cell* **34**, 893-905.e8 (2018).

21. Z. Cai, Q. Shi, Y. Li, L. Jin, S. Li, L. L. Wong, J. Wang, X. Jiang, M. Zhu, J. Lin, Q. Wang, W. Yang, Y. Liu, J. Zhang, C. Gong, H. Yao, Y. Yao, Q. Liu, LncRNA EILA promotes CDK4/6 inhibitor resistance in breast cancer by stabilizing cyclin E1 protein. *Sci Adv* **9**, eadi3821 (2023).

22. J. S. Ross, J. A. Fletcher, The HER-2/neu Oncogene in Breast Cancer: Prognostic Factor, Predictive Factor, and Target for Therapy. *Oncologist* **3**, 237–252 (1998).

23. A. Lenferink, D. Busse, W. Flanagan, F. Yakes, C. Arteaga, ErbB2/neu kinase modulates cellular p27(Kip1) and cyclin D1 through multiple signaling pathways. *Cancer Res.* **61**, 6583–6591 (2001).

24. K. M. Turner, S. K. Yeo, T. M. Holm, E. Shaughnessy, J.-L. Guan, Heterogeneity within molecular subtypes of breast cancer. *Am. J. Physiol. Cell Physiol.* **321**, C343–C354 (2021).

25. C. Wallasch, F. U. Weiss, G. Niederfellner, B. Jallal, W. Issing, A. Ullrich, Heregulin-dependent regulation of HER2/neu oncogenic signaling by heterodimerization with HER3. *EMBO J.* **14**, 4267–4275 (1995).

26. D. Diwanji, R. Trenker, T. M. Thaker, F. Wang, D. A. Agard, K. A. Verba, N. Jura, Structures of the HER2–HER3–NRG1β complex reveal a dynamic dimer interface. *Nature* **600**, 339–343 (2021).

27. M. M. Moasser, The oncogene HER2: its signaling and transforming functions and its role in human cancer pathogenesis. *Oncogene* **26**, 6469–6487 (2007).

28. Y. Yarden, M. X. Sliwkowski, Untangling the ErbB signalling network. *Nat. Rev. Mol. Cell Biol.* **2**, 127–137 (2001).

29. T. Nakakuki, M. R. Birtwistle, Y. Saeki, N. Yumoto, K. Ide, T. Nagashima, L. Brusch, B. A. Ogunnaike, M. Okada-Hatakeyama, B. N. Kholodenko, Ligand-specific c-Fos expression emerges from the spatiotemporal control of ErbB network dynamics. *Cell* **141**, 884–896 (2010).

30. P. M. Burch, Z. Yuan, A. Loonen, N. H. Heintz, An extracellular signal-regulated kinase 1- and 2-dependent program of chromatin trafficking of c-Fos and Fra-1 is required for cyclin D1 expression during cell cycle reentry. *Mol. Cell. Biol.* **24**, 4696–4709 (2004).

31. U. B. Keller, J. B. Old, F. C. Dorsey, J. A. Nilsson, L. Nilsson, K. H. MacLean, L. Chung, C. Yang, C. Spruck, K. Boyd, S. I. Reed, J. L. Cleveland, Myc targets Cks1 to provoke the suppression of p27Kip1, proliferation and lymphomagenesis. *EMBO J.* **26**, 2562-2574–2574 (2007).

32. P. Dong, M. V. Maddali, J. K. Srimani, F. Thélot, J. R. Nevins, B. Mathey-Prevot, L. You, Division of labour between Myc and G1 cyclins in cell cycle commitment and pace control. *Nat. Commun.* **5**, 1–11 (2014).

33. A. B. Pardee, A restriction point for control of normal animal cell proliferation. *Proc. Natl. Acad. Sci. U. S. A.* **71**, 1286–1290 (1974).

34. J. A. Cornwell, A. Crncec, M. M. Afifi, K. Tang, R. Amin, S. D. Cappell, Loss of CDK4/6 activity in S/G2 phase leads to cell cycle reversal. *Nature* **619**, 363–370 (2023).

35. L. García-Gutiérrez, M. D. Delgado, J. León, MYC Oncogene Contributions to Release of Cell Cycle Brakes. *Genes* **10** (2019).

36. T. Lee, G. Yao, J. Nevins, L. You, Sensing and integration of Erk and PI3K signals by Myc. *PLoS Comput. Biol.* **4**, e1000013 (2008).

37. T. Nagashima, H. Shimodaira, K. Ide, T. Nakakuki, Y. Tani, K. Takahashi, N. Yumoto, M. Hatakeyama, Quantitative transcriptional control of ErbB receptor signaling undergoes graded to biphasic response for cell differentiation. *J. Biol. Chem.* **282**, 4045–4056 (2007).

38. G. D. Grant, K. M. Kedziora, J. C. Limas, J. G. Cook, J. E. Purvis, Accurate delineation of cell cycle phase transitions in living cells with PIP-FUCCI. *Cell Cycle* **17**, 2496–2516 (2018).

39. H. Imoto, M. Okada, Signal-dependent regulation of early-response genes and cell cycle: a quantitative view. *Current Opinion in Systems Biology* **15**, 100–108 (2019).

40. M. Chung, C. Liu, H. W. Yang, M. S. Köberlin, S. D. Cappell, T. Meyer, Transient Hysteresis in CDK4/6 Activity Underlies Passage of the Restriction Point in G1. *Mol. Cell* **76**, 562-573.e4 (2019).

41. S. Mueller, J. Huard, K. Waldow, X. Huang, L. A. D'Alessandro, S. Bohl, K. Börner, D. Grimm, S. Klamt, U. Klingmüller, M. Schilling, T160‐phosphorylated CDK2 defines threshold for HGF‐dependent proliferation in primary hepatocytes. *Mol. Syst. Biol.* **11**, 795 (2015).

42. Z. Liu, S. S. Venkatesh, C. C. Maley, Sequence space coverage, entropy of genomes and the

potential to detect non-human DNA in human samples. *BMC Genomics* **9**, 509 (2008).

43. J. Guo, T. Li, J. Schipper, K. A. Nilson, F. K. Fordjour, J. J. Cooper, R. Gordân, D. H. Price, Sequence specificity incompletely defines the genome-wide occupancy of Myc. *Genome Biol.* **15**, 482 (2014).

44. A. Subramanian, P. Tamayo, V. K. Mootha, S. Mukherjee, B. L. Ebert, M. A. Gillette, A. Paulovich, S. L. Pomeroy, T. R. Golub, E. S. Lander, J. P. Mesirov, Gene set enrichment analysis: a knowledge-based approach for interpreting genome-wide expression profiles. *Proc. Natl. Acad. Sci. U. S. A.* **102**, 15545–15550 (2005).

45. C. X. Ma, F. Gao, J. Luo, D. W. Northfelt, M. Goetz, A. Forero, J. Hoog, M. Naughton, F. Ademuyiwa, R. Suresh, K. S. Anderson, J. Margenthaler, R. Aft, T. Hobday, T. Moynihan, W. Gillanders, A. Cyr, T. J. Eberlein, T. Hieken, H. Krontiras, Z. Guo, M. V. Lee, N. C. Spies, Z. L. Skidmore, O. L. Griffith, M. Griffith, S. Thomas, C. Bumb, K. Vij, C. H. Bartlett, M. Koehler, H. Al-Kateb, S. Sanati, M. J. Ellis, NeoPalAna: Neoadjuvant Palbociclib, a Cyclin-Dependent Kinase 4/6 Inhibitor, and Anastrozole for Clinical Stage 2 or 3 Estrogen Receptor–Positive Breast Cancer. *Clin. Cancer Res.* **23**, 4055–4065 (2017).

46. S. Polier, R. S. Samant, P. A. Clarke, P. Workman, C. Prodromou, L. H. Pearl, ATP-competitive inhibitors block protein kinase recruitment to the Hsp90-Cdc37 system. *Nat. Chem. Biol.* **9**, 307–312 (2013).

47. A. Prat, C. M. Perou, Deconstructing the molecular portraits of breast cancer. *Mol. Oncol.* **5**, 5–23 (2011).

48. W. Ji, W. Zhang, X. Wang, Y. Shi, F. Yang, H. Xie, W. Zhou, S. Wang, X. Guan, c-myc regulates the sensitivity of breast cancer cells to palbociclib via c-myc/miR-29b-3p/CDK6 axis. *Cell Death Dis.* **11**, 760 (2020).

49. T. Holbro, R. R. Beerli, F. Maurer, M. Koziczak, C. F. Barbas 3rd, N. E. Hynes, The ErbB2/ErbB3 heterodimer functions as an oncogenic unit: ErbB2 requires ErbB3 to drive breast tumor cell proliferation. *Proc. Natl. Acad. Sci. U. S. A.* **100**, 8933–8938 (2003).

50. J. M. Mota, K. A. Collier, R. L. Barros Costa, T. Taxter, A. Kalyan, C. A. Leite, Y. K. Chae, F. J. Giles, B. A. Carneiro, A comprehensive review of heregulins, HER3, and HER4 as potential therapeutic targets in cancer. *Oncotarget* **8**, 89284–89306 (2017).

51. J. P. Alao, The regulation of cyclin D1 degradation: roles in cancer development and the potential for therapeutic invention. *Mol. Cancer* **6**, 24 (2007).

52. K. Z. Guiley, J. W. Stevenson, K. Lou, K. J. Barkovich, V. Kumarasamy, T. U. Wijeratne, K.

L. Bunch, S. Tripathi, E. S. Knudsen, A. K. Witkiewicz, K. M. Shokat, S. M. Rubin, p27 allosterically activates cyclin-dependent kinase 4 and antagonizes palbociclib inhibition. *Science* **366** (2019).

53. R. Sears, F. Nuckolls, E. Haura, Y. Taya, K. Tamai, J. R. Nevins, Multiple Ras-dependent phosphorylation pathways regulate Myc protein stability. *Genes Dev.* **14**, 2501–2514 (2000).

54. S. B. McMahon, MYC and the control of apoptosis. *Cold Spring Harb. Perspect. Med.* **4**, a014407 (2014).

55. K. Yusa, L. Zhou, M. A. Li, A. Bradley, N. L. Craig, A hyperactive piggyBac transposase for mammalian applications. *Proc. Natl. Acad. Sci. U. S. A.* **108**, 1531–1536 (2011).

56. S. Tabata, K. Matsuda, K. Nagai, Y. Izumi, M. Takahashi, Y. Motomura, A. I. Nagasato, S. Shimma, K. Moro, T. Bamba, M. Okada, Nuclear NFκB Activity Balances Purine Metabolism in Cellular Senescence, *bioRxiv* (2023)p. 2023.04.18.536673.

57. K. J. Livak, T. D. Schmittgen, Analysis of relative gene expression data using real-time quantitative PCR and the 2(-Delta Delta C(T)) Method. *Methods* **25**, 402–408 (2001).

58. M. Martin, Cutadapt removes adapter sequences from high-throughput sequencing reads. *EMBnet.journal* **17**, 10–12 (2011).

59. A. Dobin, C. A. Davis, F. Schlesinger, J. Drenkow, C. Zaleski, S. Jha, P. Batut, M. Chaisson, T. R. Gingeras, STAR: ultrafast universal RNA-seq aligner. *Bioinformatics* **29**, 15–21 (2013).

60. Y. Liao, G. K. Smyth, W. Shi, featureCounts: an efficient general purpose program for assigning sequence reads to genomic features. *Bioinformatics* **30**, 923–930 (2014).

61. M. D. Robinson, D. J. McCarthy, G. K. Smyth, edgeR: a Bioconductor package for differential expression analysis of digital gene expression data. *Bioinformatics* **26**, 139–140 (2010).

62. A Core Team (2021), *A Language and Environment for Statistical Computing. R Foundation for Statistical Computing, Vienna, Austria* (URL https://www.R-project.org/.).

63. G. Korotkevich, V. Sukhov, N. Budin, B. Shpak, M. N. Artyomov, A. Sergushichev, Fast gene set enrichment analysis, *bioRxiv* (2021)p. 060012.

64. A. M. Bolger, M. Lohse, B. Usadel, Trimmomatic: a flexible trimmer for Illumina sequence

data. *Bioinformatics* **30**, 2114–2120 (2014).

65. B. Langmead, S. L. Salzberg, Fast gapped-read alignment with Bowtie 2. *Nat. Methods* **9**, 357–359 (2012).

66. *Picard* (http://broadinstitute.github.io/picard).

67. F. Ramírez, D. P. Ryan, B. Grüning, V. Bhardwaj, F. Kilpert, A. S. Richter, S. Heyne, F. Dündar, T. Manke, deepTools2: a next generation web server for deep-sequencing data analysis. *Nucleic Acids Res.* **44**, W160-5 (2016).

68. S. Heinz, C. Benner, N. Spann, E. Bertolino, Y. C. Lin, P. Laslo, J. X. Cheng, C. Murre, H. Singh, C. K. Glass, Simple combinations of lineage-determining transcription factors prime cis-regulatory elements required for macrophage and B cell identities. *Mol. Cell* **38**, 576–589 (2010).

69. S. Durinck, P. T. Spellman, E. Birney, W. Huber, Mapping identifiers for the integration of genomic datasets with the R/Bioconductor package biomaRt. *Nat. Protoc.* **4**, 1184–1191 (2009).

70. T. L. Bailey, J. Johnson, C. E. Grant, W. S. Noble, The MEME Suite. *Nucleic Acids Res.* **43**, W39-49 (2015).

71. J. A. Castro-Mondragon, R. Riudavets-Puig, I. Rauluseviciute, R. B. Lemma, L. Turchi, R. Blanc-Mathieu, J. Lucas, P. Boddie, A. Khan, N. Manosalva Pérez, O. Fornes, T. Y. Leung, A. Aguirre, F. Hammal, D. Schmelter, D. Baranasic, B. Ballester, A. Sandelin, B. Lenhard, K. Vandepoele, W. W. Wasserman, F. Parcy, A. Mathelier, JASPAR 2022: the 9th release of the open-access database of transcription factor binding profiles. *Nucleic Acids Res.* **50**, D165–D173 (2022).

72. L. Garcia-Alonso, C. H. Holland, M. M. Ibrahim, D. Turei, J. Saez-Rodriguez, Corrigendum: Benchmark and integration of resources for the estimation of human transcription factor activities. *Genome Res.* **31**, 745 (2021).

Main figures

Figure 1

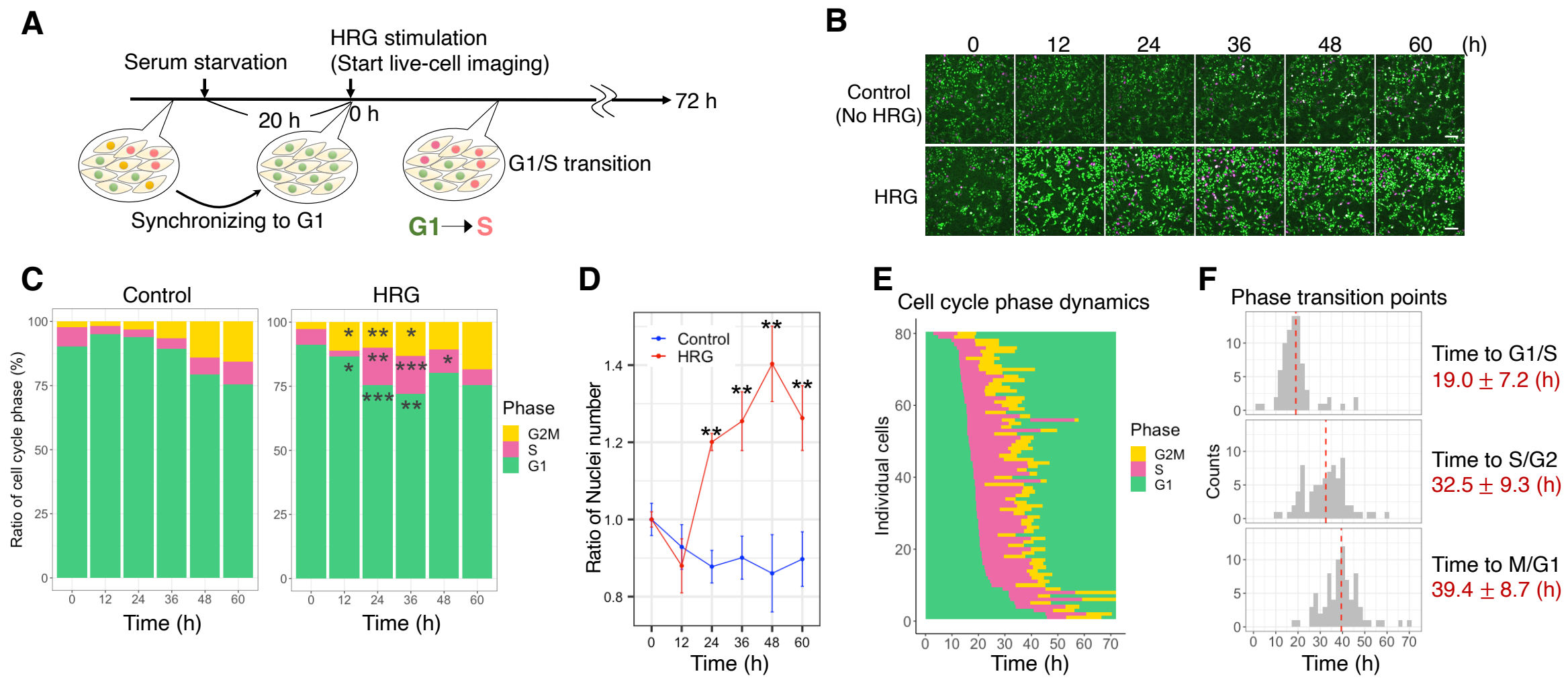

Fig. 1 Most G1/S transition events were observed approximately 20 h after ligand stimulation. (A – F) FUCCI stably expressing MCF-7 cells were used. (**A**) Experimental scheme for live-cell imaging using the FUCCI biosensor. (**B**) Images were captured every 20 min up to 72 h in conditions with or without 10 nM HRG. Scale bar: 100 µm. (**C**) Percentage distribution of each cell-cycle phase (%) in each image; n = 3 for each image quantified. (**D**) The number of nuclei increased with each passing hour relative to the cell number at 0 h. (**E**) Cell-cycle phase dynamics estimated based on Geminin and PIP fluorescence over time for each individual cell that could be followed up to 72 h; n = 79. (**F**) Histogram of each cell-cycle transition time for n = 77 cells that completed the cell cycle within 72 h, based on the results in (E). Red dotted lines indicate the mean ± SE of each transition time. In (C) to (D), *P < 0.05, **P < 0.01, ***P < 0.001 (with respect to control and HRG; t-test).

Figure 2

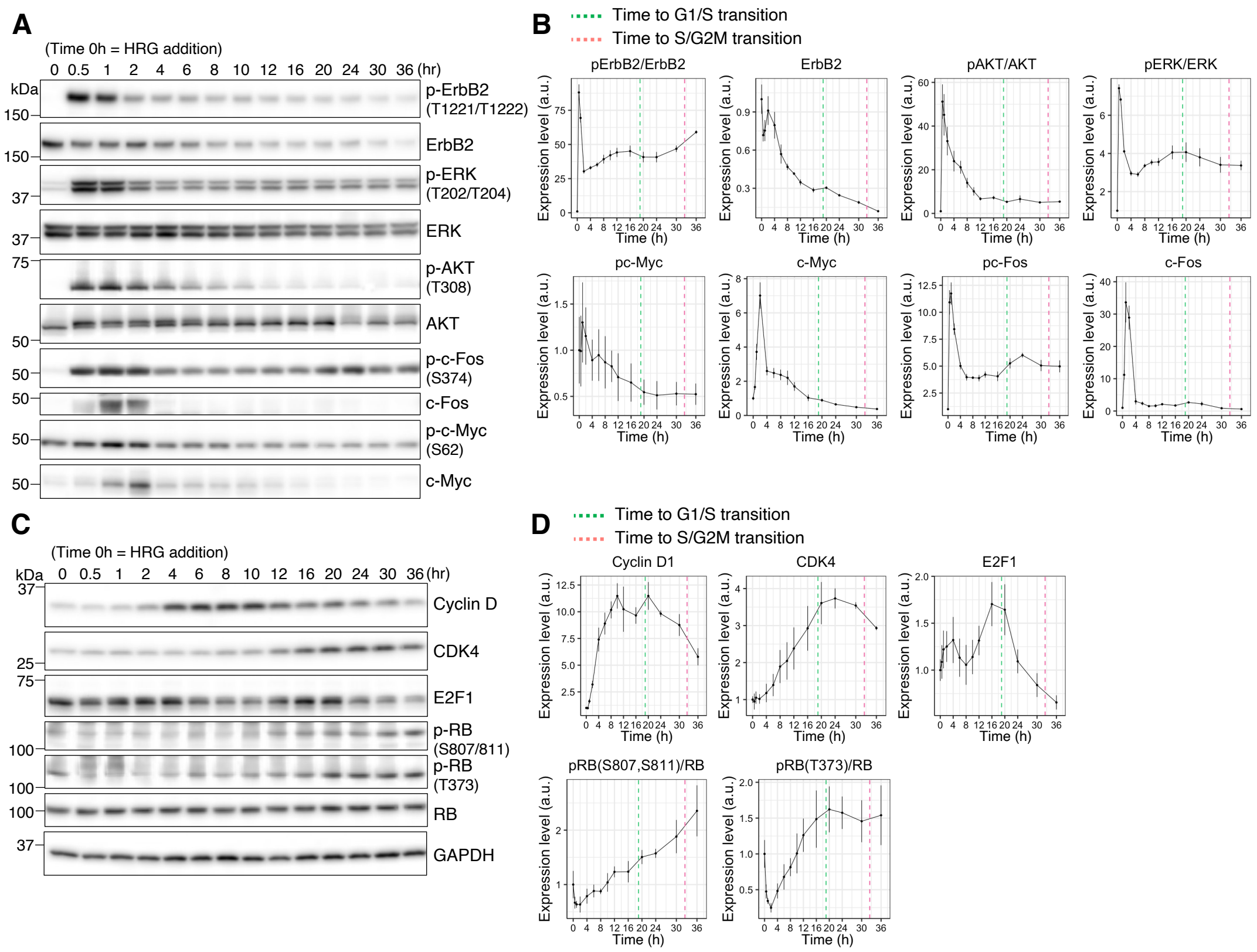

Fig. 2. Sufficient CDK4 and cyclin D1 expression is observed near the time of G1/S transition. (**A–D**) FUCCI stably expressing MCF-7 cells were used. Dynamics of changes in the expression or phosphorylation of individual proteins were detected by western blotting; (**A, B**) upstream regulatory proteins (up to transcription factors); (**C, D**) proteins regulating the G1/S transition in the ErbB pathway up to 36 h after treatment with 10 nM HRG. The expression and phosphorylation levels of each protein were normalized relative to those of GAPDH; $n = 3$. .

Figure 3

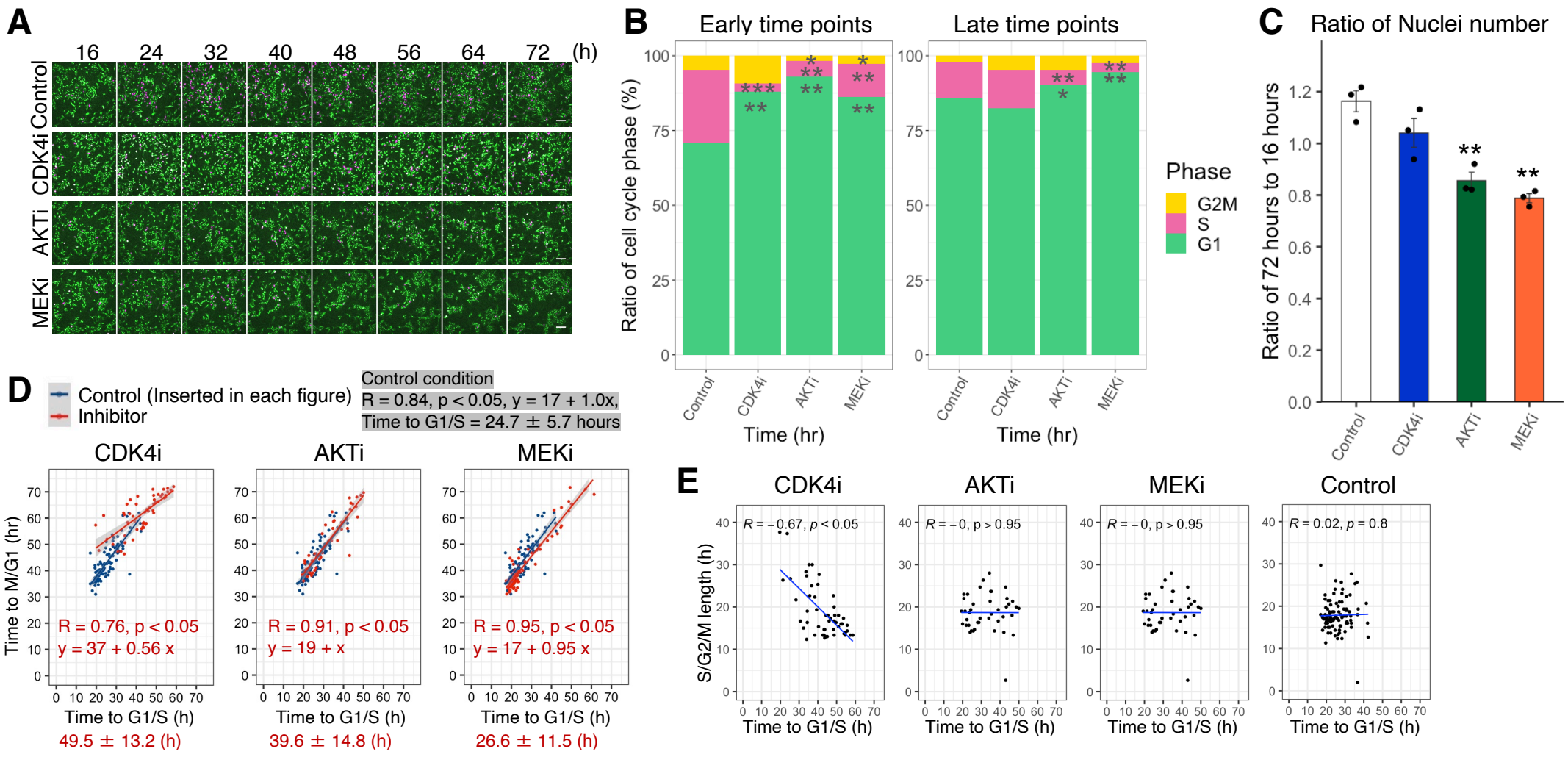

Fig. 3. CDK4 inhibition enriches a subpopulation of cells with prolonged time to G1/S transition. (**A**) Each inhibitor (250 nM CDK4i; 600 nM AKTi; 500 nM MEKi) was used to treat FUCCI stably expressing MCF-7 cells 12 h after HRG stimulation. Images were acquired every 20 min from 16 to 72 h after HRG stimulation. Scale bar: 100 µm. (**B**) Percentage distribution of each cell-cycle phase (%) in the overall image at early (32 h after HRG stimulation) and late (72 h after HRG stimulation) time points; $n = 3$. (b) The number of nuclei increased from 16 h to 72 h after HRG stimulation; $n = 3$. (**D**) Data from cells that completed the M/G1 transition within 72 h; $n = 100$ single cells were tracked. Control; $n = 96$, CDK4i; $n = 52$, AKTi; $n = 42$, MEKi; $n = 75$. Time to G1/S and M/G1 transition is shown on the x-axis and y-axis, respectively, with slope (s) and intercept (i) obtained from the regression equation. (**E**) Comparison of Pearson coefficients using data from cells used in the analysis in (D), with the time to G1/S transition plotted on the x-axis and time to the S/G2/M phase plotted on the y-axis. In (B) to (C), *$P < 0.05$, **$P < 0.01$, ***$P < 0.001$ (with respect to control and each inhibitor condition; *t*-test).

Figure 4

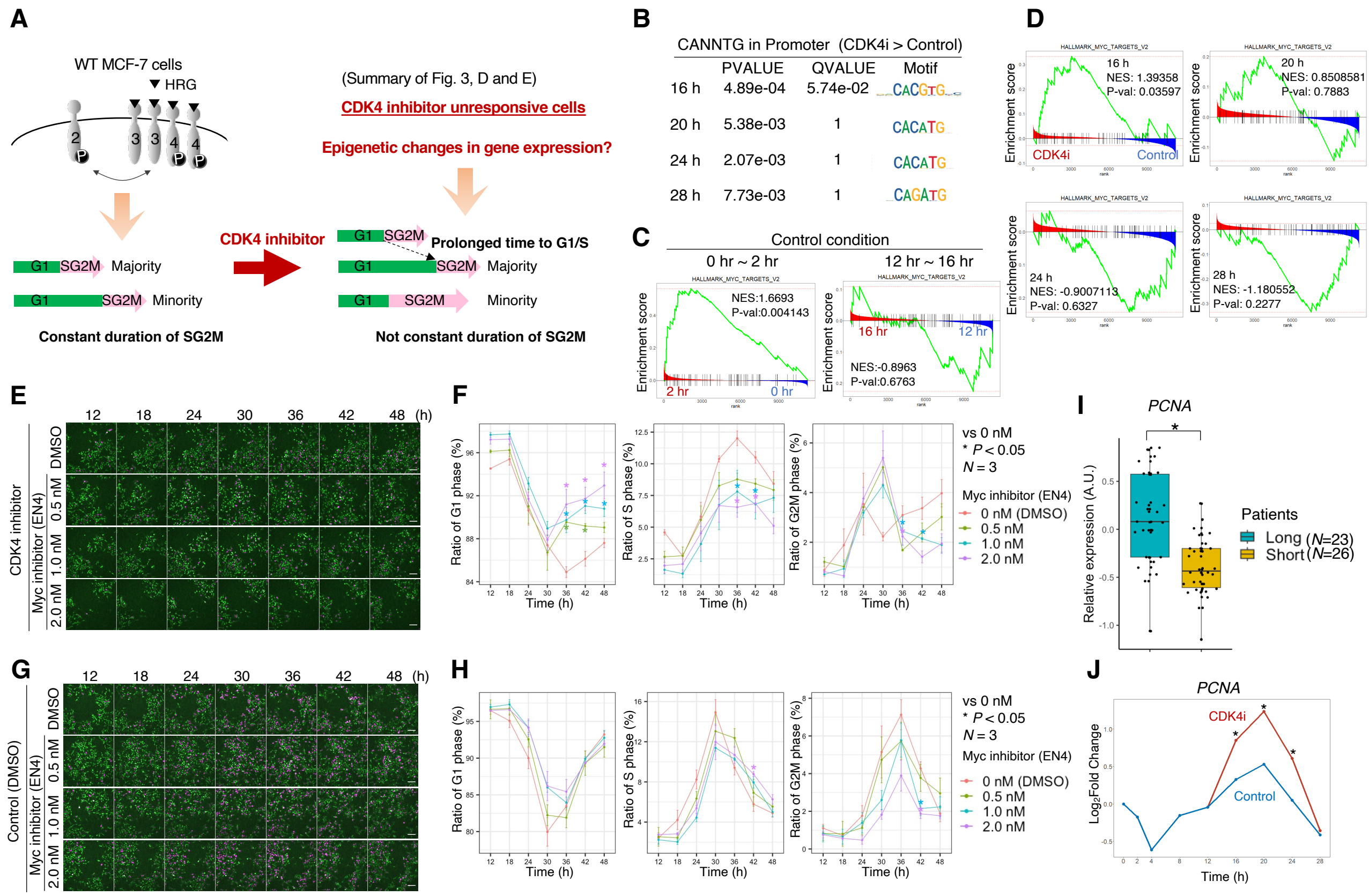

Fig. 4. CDK4is enhance the transcriptional activity of c-Myc. (**A**) Changes in cell-cycle distribution following CDK4 inhibition. (B-H, J) FUCCI stably expressing MCF-7 cells were used. (**B**) Motif-enrichment analysis of H3K27Ac modifications in the promoter region; E-box sequences (CANNTG) were enriched in the promoter region at all time points in the CDK4i-treatment group compared to controls. (**C**) GSEA was performed using the Myc-target gene set (n = 58) obtained from the Human MSigDB Collections. Comparison between 0–2 h after HRG stimulation (NES = 1.6693, P = 0.004143) and near the R point (12–16 h; NES = -0.8963, P = 0.6763). (**D**) GESA was performed using the Myc-target gene set (C). Comparison between CDK4i and control conditions every 4 h of CDK4i treatment (16 h: NES = 1.39358, P = 0.03597; 20 h: NES = 0.8508581, P = 0.7883; 24 h: NES = -0.9007113, P = 0.6327; 28 h: NES = -1.180552, P = 0.2277). (**E–H**) Conditions 11.5 h after 10 nM HRG stimulation and treatment with 0 (DMSO)/0.5/1.0/2.0 nM EN4 for 30 min. Subsequently, these MCF-7 cells were treated with 250 nM CDK4i. Scale bar: 100 µm. (**E**, **F**) or DMSO (control) (**G, H**), and the percentage distribution of each cell-cycle phase over time was quantified. (I) PCNA expression was analyzed using microarray data from luminal A subtype of breast cancer patients treated with CDK4/6i for the long term (16 weeks, n = 23) or short term (4 weeks, n = 26) (adj. P-value = 0.000132). (**J**) Expression of *PCNA* mRNA using RNA-seq data. In (F) and (H), *P < 0.05 (with respect to control and each inhibitor condition; t-test). In (I), *P < 0.05 [P-values calculated using the Benjamini–Hochberg method for controlling the false discovery rate in GEO2R]. In (J), *P < 0.05 (P-values were calculated using edgeR).

Figure 5

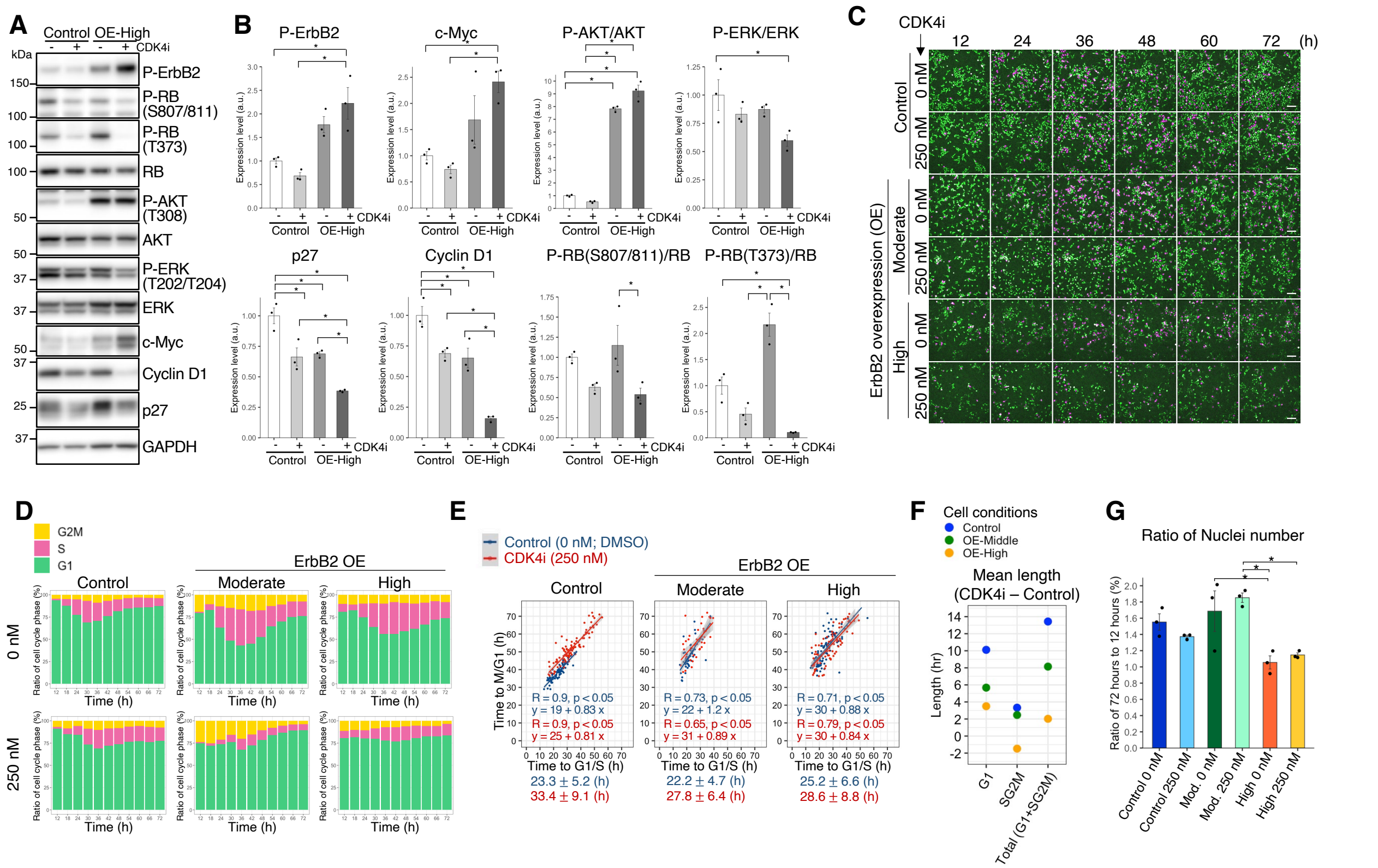

Fig. 5. ErbB2 expression induces cell-cycle arrest after CDK4 inhibition. (**A, B**) Control and ErbB2-overexpressing MCF-7 cells (high levels) were treated with CDK4i or DMSO 12 h after HRG stimulation and then harvested at 24 h post-HRG stimulation. Western blotting results (A) showing p-ErbB2, p-RB ($Ser^{807/811}$), p-RB (Thr^{373}), RB, p-AKT (Thr^{308}), AKT, p-ERK (Thr^{202}/Thr^{204}), ERK, c-Myc, cyclin D1, and p27 expression (in control cells, i.e., DMSO treatment) after normalization with GAPDH (B). (**C**) Control and ErbB2-overexpressing cells (moderate and high levels) were individually treated with 250 nM CDK4i or DMSO (no treatment) 12 h after stimulation with 10 nM HRG, and images were acquired every 20 min until 72 h after HRG stimulation. Scale bar: 100 µm. (**D**) Images in (C) were analyzed to quantitatively determine the proportion (%) of each cell-cycle phase in the entire set of images; $n = 3$. (**E**) Cells that completed the M/G1 transition within 72 h out of the $n = 100$ individually tracked cells were used. Control cells; CDK4i $n = 92$, DMSO $n = 94$, ErbB2 OE-Moderate cells; CDK4i $n = 53$, DMSO $n = 88$, ErbB2 OE-High; CDK4i $n = 81$, DMSO $n = 91$, with the time to G1/S transition plotted on the x-axis and the time to M/G1 transition plotted on the y-axis. The slope (s) and intercept (i) obtained from the regression equation are shown. The red and blue colors indicate the CDK4i and DMSO treatments, respectively. The mean ± SE time taken to reach the respective time to G1/S transition is shown at the bottom of the graph. (**F**) Using the same data as in E, the time to reach the G1/S transition (G1), the duration of the S/G2/M phase (SG2M), and the overall cell-cycle length (G1+SG2M) were assessed for differences in mean time between the CDK4i and DMSO conditions. (**G**) The number of nuclei increased from 16 h to 72 h after HRG stimulation; $n = 3$). In (B) and (G), $*P < 0.05$ (Tukey test).

Figure 6

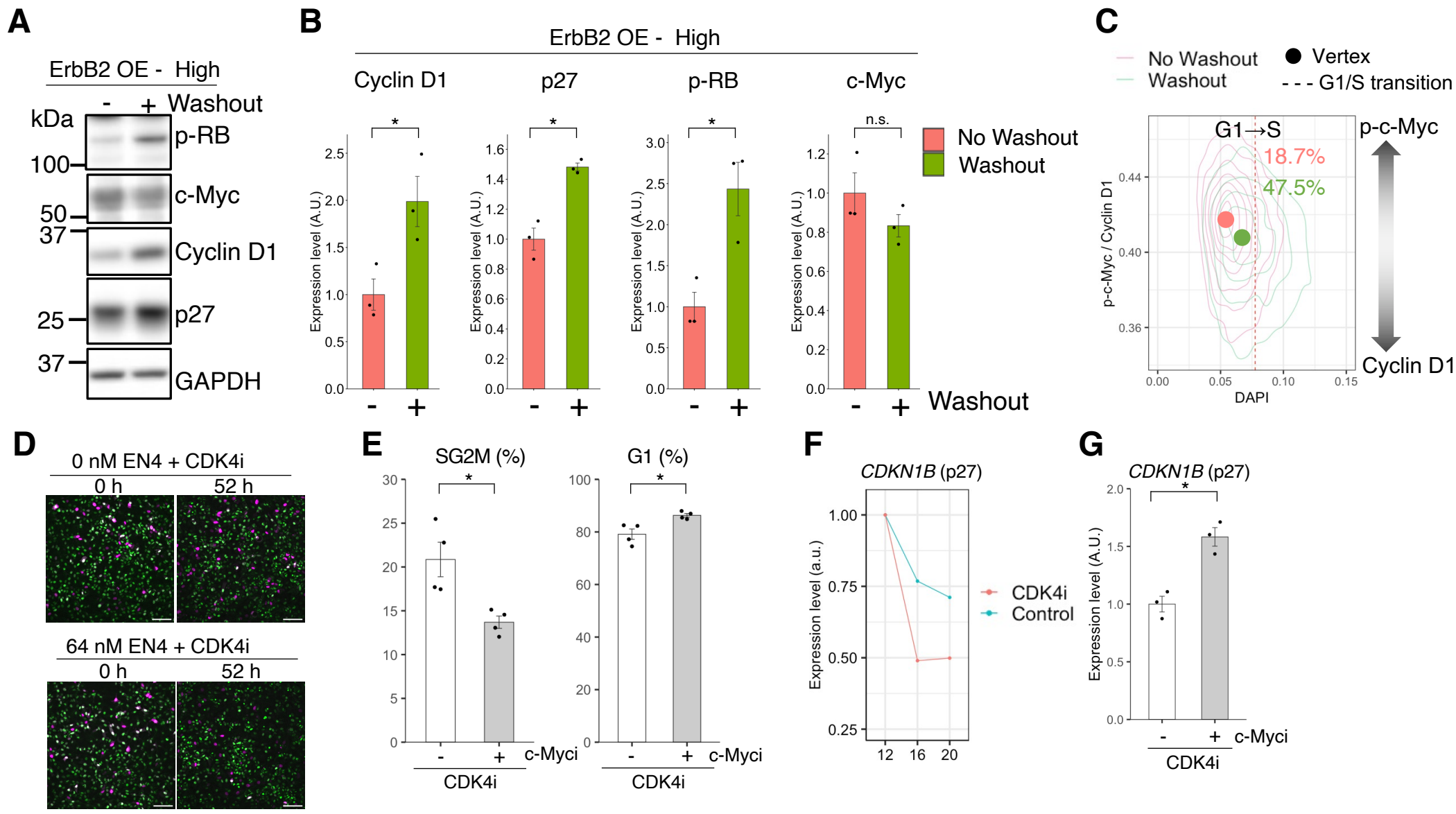

Fig. 6. Reversible cell-cycle arrest is maintained by c-Myc transcriptional activity. (**A–G**) (**A - G**) MCF-7 cells overexpressing ErbB2 (high levels) were used. (**A, B**) The following conditions were used: treatment with 250 nM CDK4i 12 h after HRG stimulation, followed by wash/no-wash treatment 4 h later; cells were harvested 40 h after HRG stimulation. Western blotting results showing the expression of p-RB, c-Myc, cyclin D1, p27, and GAPDH. After individually normalizing the proteins relative to GAPDH, the ratio to the no-wash condition was quantified; $n = 3$. (**C**) Washing operations were performed under the same conditions as in (A, B); cells were fixed 40 h after HRG stimulation and immunostained with p-c-Myc and cyclin D1 antibodies together with DAPI; $n = 3{,}859$. The x-axis shows the fluorescence intensity of DAPI, and the y-axis shows the p-c-Myc/cyclin D1 ratio. A higher value on the y-axis indicates that the amount of p-c-Myc in one cell was greater than that of cyclin D1. The black circle shows the vertex of each histogram, and the red dotted line indicates the G1/S transition time point. (**D, E**) Cells were treated for 30 min with/without 64 nM c-Myc inhibitor (EN4) 11.5 h after HRG stimulation. The cells were then incubated with 250 nM CDK4i for 8 h, washed, and imaged 52 h later (72 h after HRG stimulation; D). (**E**) The percentage distributions of G1 and S/G2/M phases were examined based on the images in (D); $n = 3$. Scale bar: 100 µm. (**F**) Twelve hours after HRG stimulation, the cells were treated with 250 nM CDK4i or DMSO (control). mRNA levels of p27 up to 20 h after HRG stimulation were examined by qPCR. (**G**) After the cells were treated with or without EN4 under the same conditions as in (D–E), RNA was collected 8 h after treatment with inhibitors, and the mRNA levels of *CDKN1B* were examined by qPCR; $n = 3$. In (B), (E), (G), $^*P < 0.05$ (*t*-test).

Figure 7

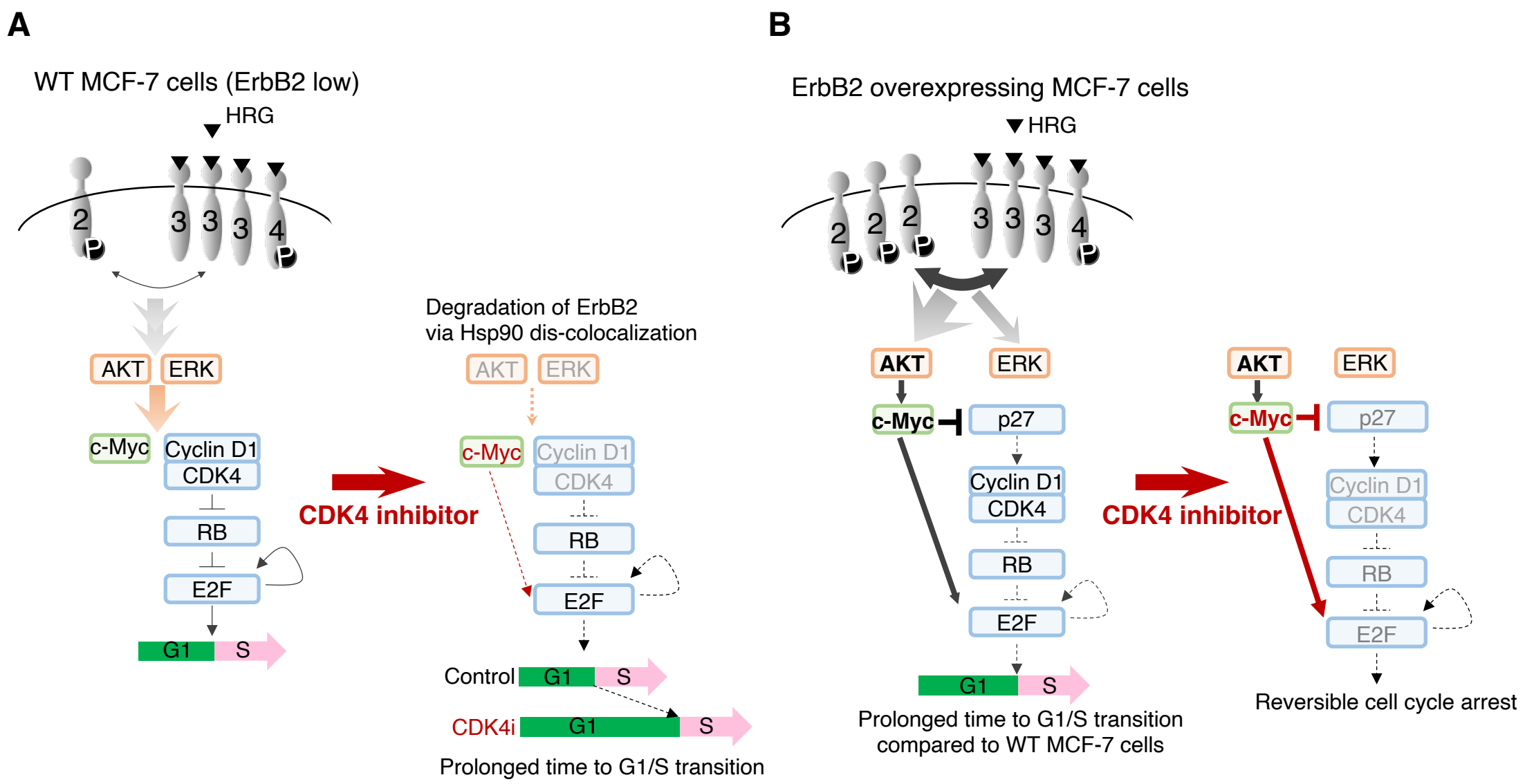

Fig. 7. Proposed model of ErbB2 modulating the ratio between cyclin D1 and c-Myc when regulating G1/S transition and altering the sensitivity to CDK4is. (**A**) In WT MCF-7 cells, the G1/S transition is facilitated by the regulation of cyclin D1/CDK4 via ERK and AKT activities. Conversely, CDK4 inhibition leads to reduced signaling activity of AKT and ERK due to ErbB2 degradation via Hsp90 dis-colocalization, leading to attenuated transcriptional activity of c-Myc activated by epigenetic changes. Consequently, a subpopulation of cells that is unresponsive to CDK4is exhibits a prolonged G1/S transition time. (**B**) In MCF-7 cells expressing high levels of high ErbB2, increased AKT activity leads to increased c-Myc expression. Subsequently, the expression of p27, which is critical for the stability of cyclin D1/CDK4 during the G1 phase, is suppressed by c-Myc, resulting in a slightly delayed G1/S entry compared to that in wild-type cells. Conversely, following CDK4 inhibition, most cells exhibit a cell-cycle arrest. This arrest is reversibly maintained by the strong transcriptional activity of c-Myc, ultimately sustaining survival signals.